2005

BONE ENGINEERING OF THE ULNA OF RABBIT

Amanda Peter Hart
University of Kentucky

ABSTRACT OF THESIS

BONE ENGINEERING OF THE ULNA OF RABBIT

Repair of bone defects is a major challenge in orthopaedic surgery. Current bone graft treatments, including autografts, allografts and xenografts, have many limitations making it necessary to develop a biomaterial to be a bone graft substitute. One such biomaterial is bioactive resorbable silica-calcium phosphate nanocomposite (SCPC). SCPC was processed using a 3D rapid prototyping technique and sintered at different temperatures to create porous scaffolds. SEM analyses and mercury intrusion porosimetry showed SCPC to be highly porous with micro- and nanopores. BET analysis indicated that SCPC had high surface area. Mechanical testing demonstrated that SCPC had a compressive strength similar to trabecular bone. Analysis of different thermal treatment temperatures indicated as the temperature was increased, the porosity decreased and the mechanical strength increased. When loaded with rhBMP-2 (SCPC-rhBMP-2), SCPC provided a sustained release profile of rhBMP-2 for 14 days. This was shown to be a greater release than hydroxyapatite (HA)-rhBMP-2. After immersion in SBF, ICP analyses showed the calcium concentration of SBF dropped drastically after one day of immersion. In conjunction, FTIR showed the formation of a hydroxyapatite layer on the SCPC surface and was confirmed by SEM. SCPC thermally treated at 850 ºC demonstrated the greatest dissolution/precipitation reactions when immersed in SBF. Processing the SCPC-rhBMP-2 hybrid using a rapid prototyping technique allowed for an exact replica of the rabbit ulna to be fabricated. This was implanted into a 10 mm segmental defect in the rabbit ulna. CT scans during the healing of the defect showed intimate union between SCPC-rhBMP-2 and the bone and about 65% healing of the defect after 4 weeks. Rabbits were euthanized after 12 and 16 weeks. Digital images show almost complete healing of the defect after 16 weeks. Torsional testing of the ulna after 12 weeks demonstrated restoration of maximum torque and angle at failure. Histological evaluation after 12 weeks showed the regenerated bone has all the morphological characteristics of mature bone. Through *in-vitro* and *in-vivo* testing, it can be recommended that the porous bioactive SCPC can serve as a successful delivery system for biological growth factors and serve as an alternative to autologous bone grafting.

KEYWORDS: tissue engineering scaffold, nanocomposite, bone morphogenetic protein-2, segmental defect, bone regeneration

Multimedia Elements Used: MPEG (.mpg)

Amanda Peter Hart

04/21/05

BONE ENGINEERING OF THE ULNA OF RABBIT

By

Amanda Peter Hart

Dr. Ahmed El-Ghannam
(Director of Thesis)

Dr. Abhijit Patwardhan
(Director of Graduate Studies)

04/21/05

RULES FOR THE USE OF THESES

Unpublished theses submitted for the Master's degree and deposited in the University of Kentucky Library are as a rule open for inspection, but are to be used only with due regard to the rights of the authors. Bibliographical references may be noted, but quotations or summaries of parts may be published only with the permission of the author, and with the usual scholarly acknowledgments.

Extensive copying or publication of the thesis in whole or in part also requires the consent of the Dean of the Graduate School of the University of Kentucky.

THESIS

Amanda Peter Hart

The Graduate School

University of Kentucky

2005

BONE ENGINEERING OF THE ULNA OF RABBIT

THESIS

A thesis submitted in partial fulfillment of the
requirements for the degree of Master of Science
in Biomedical Engineering
in The Graduate School
at the University of Kentucky

By

Amanda Peter Hart

Lexington, Kentucky

Director: Dr. Ahmed El-Ghannam, Professor of Biomedical Engineering

Lexington, Kentucky

2005

DEDICATION

This thesis is dedicated to my mom for her patience and understanding for the last 24 years. She has stood by my side in thick and thin. Without her I do not think I would have gotten this far in life. I want her to know that all of my hard work is because of her. Her help and support has been invaluable and I am eternally grateful.

ACKNOWLEDGMENTS

For the last two year, the research and writing of this master's thesis has taken over my life. As much as I have fought it, it has become my life. And I am grateful for that. I have learned so much from so many great people and I would like to take this opportunity to thank them. Dr. Ahmed El-Ghannam, my thesis advisor, who never gave up on me, thank you for giving me the opportunity to work on this project and for the help and guidance that has been extended to me during the last two years. Thanks to Dr. Larry Cunningham for his surgical expertise and his abundant sense of humor. To Dr. Dean White, thank you for your help with the histology and I am sorry for always bugging you to get done. Thanks to Patty Lott at the University of Alabama-Birmingham for her help with the histology. For their help with the mechanical testing, I would like to thank Dr. Marwan Khraisheh and Fadi Abu-Farha. The DLAR staff has been great to work with and they helped out tremendously with the rabbits and the surgeries. Special thanks to Samantha Otte for all her help with the rabbits and always returning emails. I wish to acknowledge Larry Rice, "the SEM guy", for his help with my samples and the great discussions about Kentucky football. Thanks to the people at Micromeritics for analysing my samples. I want to thank the engineers at CRMS for helping process my samples. Thanks to Dr. Congqin Ning, Junaid Mehta, and Gautam Gupta for their help and patience in the lab and for teaching me so much. Thank you to Dr. David Pienkowski and Brock Marrs for letting me used their lab equipment for the torsional testing. To the wonderful Diagnostic Radiology department at UK Chandler Medical Center, thank you for the help with the CT scans and for always finding a way to squeeze us in to your busy schedule. I want to thank Spunky the rabbit, for if it wasn't for him none of this could have been possible. For his sacrifice, we were able to make this study a huge success. Thanks to Jessica Sharon for her support through all this. At times it seems like she was the only one who understood what I was going through. Congratulations to her for surviving all this along side of me. Finally, I owe all of my achievements to my family, my mom Pam Hart, my sisters Stacy McClure and Jody Osisek, and my nieces and nephew Emilee, Nathaniel, and Kristina McClure. Without their support, I would not have been able to complete this thesis.

TABLE OF CONTENTS

LIST OF TABLES

LIST OF FIGURES

Chapter 1

Introduction

1.1 Bone Grafts

Skeletal deficiencies that result from trauma, tumors or abnormal development frequently require surgical intervention in order to restore normal tissue function [1]. In the US alone there are over 2.2 million orthopaedic procedures performed each year, 450,000 of those being bone graft procedures. This makes bone the most common tissue for transplant procedures, second only to blood [2]. Although current surgical treatments are often successful in repairing bone defects, they all have problems and limitations.

Bone grafts are needed when part of your body is missing bone. This missing portion of bone is frequently called a bone defect. A bone graft is a surgical procedure that replaces the bone defect with material from the patient's own body or an artificial, synthetic, or natural substitute. The purpose of the graft is not only to replace the missing bone, but also to stimulate new bone formation in the bone defect area [3]. The graft forms a bridge and acts a scaffold in the defect area until new bone can grow in its place. Eventually the newly formed bone should completely replace the bone graft material.

1.1.1 Autografts

Currently there are three main types of biological bone graft procedures. The first is the autograft, the "gold standard" method for repairing bone [3]. This is where bone is harvested from a patient's own body, typically from the pelvis or iliac crest. Autogenous bone grafts provide both osteoinductive and osteoconductive stimuli for bone growth. They can be used to not only provide mechanical support but also to stimulate new bone formation. Autogenous bone grafting has excellent fusion rates and has become the

standard by which all other bone grafts are measured. Many surgeons prefer autogenous bone grafts because there is no risk of the body rejecting the graft since it came from the patient's own body. However, the success of the autograft is often compromised due to its many limitations. These include the fact that removing bone from one part of the body creates the same deficit there as in the area being repaired, possible donor site morbidity, limited donor bone supply, anatomical and structural problems, high costs, and the need for multiple surgeries [3].

1.1.2 Allografts and Xenografts

In an effort to minimize the problems associated with taking the patient's own bone, a common alternative to the autograft is the use of allograft or xenograft bone. An allograft bone graft is bone harvested from deceased individuals who have donated their bone for use in the treatment of living patients. The advantage of the allograft is that multiple surgeries within the same patient are not required. However, the shortcomings greatly outweigh the benefits [2]. The downfalls to the use of allografts are the necessity of having compatibility between donor and recipient, it does not promote bone growth very well, there is limited donor supply, and diseases may be transmitted together with the implant [4].

The third type of biological bone graft is the xenograft. A xenograft is a graft in which bone tissue is taken from another species. Xenografts are biocompatible and are also osteoinductive in nature. Contrary to the auto- and allograft, xenografts are available in almost endless supply. However, like allografts, xenografts have problems with compatibility between donor and recipient, and possible disease transmission.

1.1.3 Synthetic Grafts

In order to offer the advantages of the autograft, allograft, and xenogaft and eliminate the limitations, it is necessary to develop a biomaterial to be used as a bone graft substitute.

1.1.3.1 Bioceramics

Bioceramics, such as hydroxyapatite (HA), tricalcium phosphate (TCP), and bioactive glass (BG), are one type of biomaterial that is being used as synthetic bone grafts. These synthetic materials have similar surface structure to that of natural bone, making them osteoconductive. Most osteoconductive materials bond to bone and allow direct bone deposition on their surface. Synthetic porous bioceramics are primary candidates as bone substitutes due to not only their excellent osteoconductive properties, but they are available in unlimited supply, and they can have custom-designed shape and size. They are not associated with disease transmission, cause neither chronic inflammation nor systemic toxicity, and there is no foreign body response nor any evidence of rejection [5]. They are available in many forms such as porous particles and pastes [6]. Although ceramics may provide a scaffold for bone growth, they are not osteoinductive, meaning they do not have the ability to enhance osteogenic differentiation of osteoblastic cells. Also, the application of porous ceramics for load-bearing conditions is difficult due to their adverse mechanical properties; they are brittle, have low impact resistance, and have low tensile strength [5].

1.1.3.2 Polymers

Polymers such as poly(lactic) acid (PLA), poly(glycolic) acid (PGA), and their co-polymers (PLGA), and are often used as bone graft substitutes. These materials have the advantage of altering their chemical structure so that they can be integrated with growth factors, drugs, and other compounds to create delivery systems. They are biocompatible,

resorbable, can be processed into porous scaffolds that have mechanical properties similar to that of bone. However, some polymers are not osteoconductive and it has been found that as certain polymers degrade, they release acidic by-products which can inhibit new bone formation and even cause bone resorption [7, 8].

1.1.3.3 Metals

Metals are another type of synthetic biomaterial that can be used as a biomaterial for bone defects. Metals such as titanium and titanium alloys, stainless steel, and cobalt-chromium have been widely used in the orthopaedic field and can be utilized in load-bearing conditions. This is due to their excellent mechanical characteristics in terms of stiffness and elasticity and bone compatibility [9]. Conversely, most metals are not osteoconductive, and none are osteoinductive, or resorbable.

1.1.3.4 Composites

Composite bone grafts are the combination of multiple biomaterials. These are used in order to maximize the advantages and minimize the limitations of these synthetic graft materials. Such combinations of these include ceramic-metal, ceramic-polymer, ceramic-ceramic. In combining a ceramic with a metal, the composite can have the mechanical strength of a metal while taking on the osteoconductive property of a ceramic. By combining a ceramic with a polymer, the structure of the biomaterial is less brittle than a ceramic alone and the polymer can become osteoconductive. Combining different biomaterials can create a composite that is porous, resorbable, biocompatible, osteoconductive, and has good mechanical strength. Yet, in developing a biomaterial as a bone graft substitute it is not only necessary to fill the bone defect with an osteoconductive scaffold, but to seed that scaffold with osteoinductive growth factors that will stimulate new bone tissue to grow in and around the porous scaffold.

1.2 Tissue Engineering

Tissue Engineering is a multidisciplinary field that combines the principles of biology and engineering to develop tissue substitutes to restore, maintain, or improve the function of diseased or damaged tissues, such as bone. Cytokine therapy is one area of bone tissue engineering that involves seeding highly porous, biodegradable scaffolds with growth factors, then implanting the scaffolds to induce and direct the growth of new, healthy bone at a target site [10, 11]. For a scaffold to be used as a tissue engineering scaffold it should fulfill three primary purposes [12]. First, it should geometrically replicate the size and shape of the defect. Second, it should temporarily fulfill the physical function of the bone tissue it is replacing. Finally, the scaffold material composition and porous microstructure should enhance tissue regeneration.

1.2.1 Growth Factors

Growth factors, such as bone morphogenetic proteins (BMPs) and transforming growth factors (TGF-β), are osteoinductive agents that occur naturally in bone. Growth factors are very powerful stimulants for bone formation and can be used alone or with a carrier system as graft replacements. These biologically active proteins play a key role in the body's own natural bone-forming process and are found naturally at sites of bone fracture. These proteins can be produced, concentrated and placed in the body in areas where bone formation is needed and are powerful enough to stimulate bone formation without the need for taking the patient's own bone.

BMPs are a subgroup of factors in the TGF-β superfamily and consist of a family of at least 15 structurally related osteoinductive growth factors. They were originally identified as protein regulators of cartilage and bone formation. There are several different BMPs naturally found in the body and many play a critical role in bone formation. The most promising proteins are BMP-2 and BMP-7 [13]. These two proteins have been extensively studied in animals and humans with very promising results [14].

Both proteins have shown to successfully stimulate new bone formation in defect sites and with higher success rates when used alone as compared to using the patient's autogenous bone graft. They accomplish this by inducing differentiation of stem cells into osteogenic bone forming cells.

Recombinant human bone morphogenetic protein-2 (rhBMP-2) is a substance that was cloned by Wozney et al. [15]. rhBMP-2 stimulates the expression of differentiation markers of osteoblasts *in-vitro* [16] and initiates a complex series of cellular events culminating in bone formation [17]. Although BMP can induce bone formation at a defect site alone, due to its short half-life, rapid diffusion and degradation [16] the dose needed to induce this bone formation can be quite high. This dose can be greatly reduced when BMP is combined with an appropriate biodegradable scaffold carrier that can immobilize the protein while retaining its bioactivity [18]. In addition to reducing the dose needed for bone induction, a carrier acts as a means of deployment for BMP. By attaching BMP to a delivery system, the bioactivity of the protein can be maintained for a longer period of time and the protein can be held in place at the target site [11]. A carrier must not inhibit the bone formation and bone repair capability of the BMP [11]. When used with a biomaterial carrier system, BMP has been shown to stimulate bone formation, alkaline phosphatase activity, collagen synthesis, and osteoblast differentiation [19].

1.2.2 Ideal Characteristics of BMP Carrier

One of the major functions of a delivery system for BMPs is to retain BMP at the grafted site for a period of time sufficient to induce bone [20] so that the molecules can exert their biological action. Therefore, a carrier should have controlled release kinetics of BMP, meaning it has the ability to deliver the growth factor at the appropriate time and in the proper dose [14].

Another major function is to provide an initial substratum for the growth and differentiation of bone-forming cells. In order to be this initial substratum, a bone tissue engineering scaffold must possess certain characteristics. First of all, the tissue engineered scaffold should be biocompatible and not elicit an inflammatory or immunogenic response in the body [20].

An ideal biomaterial carrier should also be highly porous providing a pathway of interconnections through which new cells can migrate and new blood vessels can form. If the pore size of the biomaterial exceeds 100 μm, bone will grow within the interconnecting pore channels near the surface and maintain its vascularity and long-term viability [21]. Although, for a resorbable material, the immediate resorption that takes place when it is immersed in a physiological solution will increase its pore sizes, eliminating the need for the initial porosity of the biomaterial to be specifically defined. Nevertheless, the implant should serve as a scaffold for bone formation, maintaining surface area and volume to facilitate directional bone formation [22]. A porous scaffold also provides an appropriate surface environment in which cells can adhere and proliferate.

A biomaterial also needs to be osteoconductive and have the ability to promote bone growth by allowing bone formation on its surface. Biomaterials with good osteoconductive properties can form a tight bond with the host bone tissue, a characteristic which is desirable for the restoration of bone function at a defect site [20]. The biomaterial also should be osteoinductive, stimulating new bone formation. And osteoinductive means that the material will enhance osteogenic differentiation of osteoblatic cells, the cells that will build new bone.

The biomaterial should also ideally be resorbable, so that as new bone grows, the scaffold can slowly degrade away and eventually be completely replaced by newly regenerated bone [20]. The degradation rate of the biomaterial needs to be controlled so that it does not degrade away too quickly before new bone can grow in its place, or too slowly inhibiting new bone formation. In addition, when used as a carrier for BMP, if a

biomaterial degrades too fast the BMP may be released too rapidly and the risk of fibrous ingrowth, and failure of bone healing, is increased.

In order for the biomaterial to initially replace bone, it needs to exhibit similar mechanical properties of bone [21]. If used in a load bearing situation, the scaffold needs to possess enough rigidity to be able to withstand the forces that are going to be applied to it. But there is a trade off between porosity, which is important, and mechanical strength [5]. As the porosity increases, the mechanical strength is going to decrease. There needs to be a balance between the two so that the stimulation of new bone formation can be greatest.

Because no bone in the body is a perfect cylinder of rectangle, the geometry of the scaffold must also be appropriate for the implantation site, as it will define the area in which the bone is formed [11]. A precise geometry is not only important in order to achieve maximum restoration of function, but also for cosmetic reasons as well. This is especially true for maxillofacial bone graft procedures. In addition, since the size and shape of an implant can influence the degradation rate of the carrier, the rate of release of BMP, and the bonding of bone to the implant, it is essential to have a scaffold that is the exact shape of the specific bone defect that it is temporarily replacing.

1.2.3 Current BMP Carriers

1.2.3.1 Collagen

The most common scaffold materials used as BMP carriers include collagen and biodegradable polymers [9, 23].

Collagen is a fibrous protein that is abundantly found in the extracellular bone matrix. The porous structure of collagen makes it conducive to mineral deposition, vascular ingrowth, and growth-factor binding. This structure provides both a physical and

chemical environment that is favorable to new bone regeneration. Absorbable collagen sponges have served as carriers for growth factors, limiting the diffusion of rhBMP-2 through collagen-rhBMP-2 interactions and physical trapping [24]. These interactions have assisted in establishing a prolonged release of BMP at the target site. However, collagen provides little or no initial structural support and has potential immunogenicity [2].

1.2.3.2 Polymers

Polymers are biomaterials that have been applied in clinical practice in fracture fixation for over 20 years. The most popular of the polymers used are PLA, PGA, and PLGA. Because of their biocompatibility and their ability to bind proteins, polymers have been widely used as scaffolds to deliver BMP. Polymers are a promising material for BMP delivery since their chemical structure, and thus its release kinetics of BMP, can be easily altered. Polymers can be made into porous, resorbable scaffolds that have the proper mechanical strength in order to replace bone. One study reported that encapsulation of BMP with a biodegradable PLGA is an effective polymeric vehicle for the controlled release of BMP [1]. However studies have shown that as some polymers degrade, isolated areas of fragmentation and degradation of the polymer scaffold had elevated areas of inflammatory response cells [7, 8]. As polymers degrade they can release acidic by-products that have adverse foreign body reactions.

1.2.3.3 Calcium Phosphates

Another major group of biomaterials that are used as carriers for BMP delivery are calcium phosphate-based bioceramics. Calcium phosphates have been used in medicine and dentistry for nearly 30 years [22]. They are widely used as bone substitutes due their high bioactivity. They have been known to easily bond to bone and enhance bone tissue formation. Calcium phosphates can be classified as non-resorbable or resorbable. Two of the forms of calcium phosphate ceramics that are most widely used are TCP and HA.

Both have similar structures to that of bone and have been shown to be osteoconductive [25]. Calcium phosphate ceramics can be processed to be porous scaffolds and because of this have been widely used as tissue engineering scaffolds for the delivery of growth factors [21, 26-29]. One study investigated a porous calcium phosphate ceramic with micro-porous structures, which consisted of HA and a trace of α-TCP, as a BMP carrier [29]. Mature lamellar bone was found in the implants after 35 days, indicating the calcium phosphate ceramic was an effective carrier of BMP.

Unfortunately, calcium phosphate ceramics also exhibit many limitations. When calcium phosphate ceramics have been used as carriers for BMP delivery they have often elicited inflammatory and immunologic reactions [30]. It has been found that porous TCP ceramics are dissolved and resorbed relatively quickly and do not have good mechanical stability [5]. Moreover, this adversely high-dissolution rate has been associated with an elicited immunologic response [31]. As for HA, although it has been shown that bone does grow in porous and dense HA particulates, the bone conductivity is limited [25]. The major limitation in using calcium phosphate ceramics is their poor mechanical properties. They have been shown to be brittle, so when implanted in place of bone there is minimal immediate structural support.

1.2.3.4 Bioactive Glasses

Bioactive glass is another calcium-phosphate based bioceramic used to replace bone that can be considered as a BMP carrier. Besides being composed of calcium and phosphorus, another major component is silica. Due to its amphorous structure, it is known to have a stimulatory effect on bone cell function, making it a favorable bioactive biomaterial. As compared to HA, BG accelerated bone growth 3 times more when implanted in bone [32]. Bioactive glasses form a tight bond with surrounding tissues by the *in-vivo* formation of a biologically active carbonate-containing hydroxyapatite layer (HCA) on the glass surface. However, BG is a solid non-resorbable material [33]. Therefore, when synthesized as a nonporous carrier for the delivery of BMP, the growth

factors can only be seeded onto the outside of the BG scaffold. Upon implantation this would cause an immediate release of all the protein. As discussed before an appropriate carrier would retain the BMP at the grafted site for a period of time sufficient to induce bone.

1.2.3.5 Composites

Now the previously mentioned carriers all had different characteristics that set them apart as possible delivery systems for BMP. But none of them seemed to have all of the qualities necessary to make them that perfect tissue engineering scaffold for BMP delivery. A composite graft can combine different carriers so that the weaknesses of one are overridden by the strengths of another. One example of a composite graft could combine an osteoconductive biomaterial with a biomaterial that provides good mechanical properties, potentially replicating bone functionality. One study combined a titanium mesh and calcium phosphate ceramic [27]. The titanium mesh provided the composite with excellent mechanical properties and biocompatibility. The calcium phosphate coated the titanium mesh and provided the osteoconductivity to the composite. Another example of a composite could be a polymer-ceramic composite. A study combined the synthetic biodegradable polymer PLA with interconnected-porous calcium HA [10]. This composite combined the strength of the polymer with the osteoconductivity of the ceramic. When implanted in a critical sized defect, the composite graft induced new bone formation in the pores and around the implant with sufficient strength and anatomical structure.

1.2.3.5.1 Silica-Calcium Phosphate Composite

Another composite biomaterial is the one being used in this study. This composite biomaterial has been developed to possess all of the characteristics needed in order to be a tissue engineering scaffold for BMP delivery and bone regeneration. This material is SCPC or silica-calcium phosphate composite. This biomaterial is resorbable, porous, and

bioactive. Previous studies in our lab have shown that SCPC has superior stimulatory affects on bone tissue regeneration when compared to BG or HA ceramic. Moreover, when the material was used as a carrier for BMP, the SCPC-rhBMP-2 hybrid provided a sustained release profile of biologically active rhBMP-2 and enhanced mesenchymal stem cell differentiation and bone tissue formation in-vitro.

1.3 Processing and Fabrication of Tissue Engineering Scaffolds

Once a biomaterial is found that meets all of the qualifications of a tissue engineering scaffold for BMP delivery and bone regeneration, it must be processed into a scaffold. For bone tissue engineering, the bone graft substitute needs to have adequate porosity for bone repair so as to accelerate bone regeneration. The scaffold must also replicate the size and shape of the defect it is going to fill. Both of these characteristics synergistically play an integral role in the success of the bone substitute. And accurate repair of bone defects is not only important in obtaining restoration of bone function but is also important for cosmetic reasons as well. This is especially true for maxillofacial bone reconstructions. Yet many studies that have engineered biomaterials to fill irregular bone defects use cylinders or blocks [10, 23, 26, 31, 34].

Traditional processing of biomaterials has demonstrated scaffolds with limited control over geometry and porosity. These include polymer foaming technique, particulate-leaching, solid–liquid phase separation, textile technique, and extrusion process [35]. These primitive methods create scaffolds which are cylinders, blocks, particles or pastes. The structure of these types of scaffolds does not mimic that of bone, which is essential to vascularization and tissue regeneration.

1.3.1 Rapid Prototyping Technologies

The novel technologies of solid freeform (SFF) or rapid prototyping (RP) are becoming the choice for scaffold processing, due to the ability to engineer scaffolds with predefined

and reproducible internal morphology that replicates that of natural bone. SFF technologies involve designing a scaffold model with 3D computer aided design (CAD) or obtaining data originating from computed tomography (CT) or magnetic resonance imaging (MRI). This digital information can then be converted to a machine specific cross-sectional format, expressing the model as a series of layers. This data is then used by the SFF machine which produces a physical model in a layer-by-layer method. Through this type of processing technology, it is possible to control scaffold architecture, material composition, and porosity which are all critical factors in the development and future success of tissue engineering.

1.3.1.1 Fused Deposition Modeling

Currently, there are only a few SFF techniques that are being used for scaffold processing. One such RP technique that has been extensively researched is fused deposition modeling (FDM) [35-38]. FDM uses the concept of melt extrusion in order to deposit a parallel series of material roads that forms a material layer. For this type of scaffold fabrication, a filament material stock is fed and melted inside a heated liquefier head and then is extruded through a nozzle with a small orifice. For each deposited material layer, the direction of material deposition can be changed. By changing the direction of material deposition for consecutively deposited layers and the spacing between the material roads, scaffolds with highly uniform internal honeycomb-like structures, controllable pore morphology and complete pore interconnectivity are obtained, simulating the internal structure of bone.

1.3.1.2 Selective Laser Sintering

Another SFF technology that has been adapted for fabricating tissue engineering scaffolds is selective laser sintering (SLS) [38]. This technology utilizes a CO_2 laser beam to selectively sinter polymer or composite powders to form material layers. The laser beam is directed onto a powder bed by a high precision laser scanning system.

Subsequent stacking and fusion of the sintered material layers creates a scaffold that replicates the object's height. Due to the powders being subjected to low compaction forces during their deposition to form new layers, this technology creates objects which are porous.

1.3.1.3 Three-Dimensional Printing

The most commonly used SFF technology is three-dimensional printing (3D-P) [38]. This technique employs the technology of ink jet printing for the processing of materials in powder form. Because of the versatility and simplicity of 3D-P, it allows for the processing of a wide variety of biomaterials that include polymers, metals and ceramics. During fabrication of a scaffold, a printer head is used to print a liquid binder onto thin layers of selected powder. The binder sprays an area that is the same as the scaffold's cross-sectional area as generated by a system computer. The successive stacking and printing of material layers onto the top of previously printed layer recreates an exact replica of the desired object. After sintering this fabricated material, the binder is burned away leaving a highly porous scaffold.

1.3.1.3.1 Z-Corp Processing

One specific example of 3D-P called Z-Corp processing was used in this study. A Z-Corp 3D printer was used in order to fabricate porous disk scaffolds for *in-vitro* testing, and exact replicas of rabbit ulna segmental bone defects for *in-vivo* testing. By combining Z-Corp processing with SCPC powder, highly porous, bioactive, resorbable tissue engineering scaffolds were fabricated in only minutes. These scaffolds were processed with an adequate porosity for bone repair, and a specific geometry, replicating the size and shape of the defect it was going to fill.

1.4 Objectives

The main goal of this study was to employ a 3D processing technique with the SCPC powder to develop a tissue engineering scaffold for BMP delivery and bone regeneration in a load bearing segmental bone defect. The specific objectives were:

1 Evaluate the effect of different thermal treatment temperatures on the mechanical strength, porosity and surface area of SCPC.

2 Evaluate the effect of thermal treatment on the dissolution kinetics of the material in physiological solution.

3 Correlate the physicochemical properties of the material to the development of bioactive surface layer on the SCPC in physiological solution.

4 Study the release kinetics of rh-BMP-2 from SCPC-rh-BMP-2 hybrid in physiological solution.

5 Test the ability of the SCPC-rhBMP-2 hybrid to enhance bone regeneration in a load bearing large bone defect in the ulna of rabbit.

Chapter 2

Materials and Methods

2.1 *In-Vitro* Study

2.1.1 Sample Preparation

Table 2.1.1 shows the chemical compositions of the silica-calcium phosphate composite and hydroxyapatite (ProOsteon® 200HA) that were used in this study. Previous studies in the lab have shown that the composition of ratio 75:25 Sodium Silicate to Calcium Phosphate has high bioactivity [33]. Batches of 100 g of the composition were placed in polyethylene bottles and placed on a roller mixer and allowed to mix for 24 hours to ensure even distribution of the powders. Each batch was moistened with 0.1% NaOH until a paste was formed and spread into a prefabricated teflon mold with 10 mm diameter × 10 mm height cylindrical cutouts. The SCPC samples were left to dry at room temperature and then thermally treated (Thermolyne 30400 Furnace, Sybron/Thermolyne Corporation, IW, USA) at 100 ˚C for 1 hour and then 800 ˚C for 1 hour.

2.1.2 Z-Corp Processing

Particles in the size range 45-90 μm were prepared by grinding the SCPC using a mortle and pestle then sieving to achieve the desired particle size range. These particles were then processed using a Z-Corp 3D Printer (Z402 System, Z Corporation, Burlington, MA, USA). Z-Corp printers use a powder-binder technology to create parts directly from digital data. In order to get the desired shape to be modeled by the Z-Corp, the first step is to obtain high resolution MRI or CT data of the area of interest. This data is then converted into a stereolithography (STL) data format, which remaps the surface data to a series of triangles that when assembled reconstruct the original geometry. This

Table 2.1.1: Chemical Composition of SCPC and HA in mol %

Composite code	Na_2O	SiO_2	CaO	P_2O_5
SCPC	32.9%	32.9%	22.8%	11.4%
HA	0	0	76.9%	23.1%

file is then imported into a computer aided design (CAD) software package (Amira, Amira 3D Professional Visualization, Berlin, Germany). This step allows adjustments to the image to be made. The final CAD image is then converted back into a STL format, and then into a slice file that the Z-Corp machine will use in order to replicate the model layer by layer. The thickness of each of these layers can be 0.076 - 0.254 mm. To process the desired prototype, first the Z-Corp spreads out a thin layer of the SCPC powder (Figure 2.1.2). Then, an ink-jet print head prints a water-based binder, made of water and agar, in the cross-section of the part being created. Next, the build piston drops down, making room for the next layer, and the process is repeated. Once the part is finished, it is surrounded and supported by loose powder, which is then shaken loose from the finished part. After building the prototype, any unused powder is collected and can be reused.

In order to make SCPC disks using the Z-Corp machine for *in-vitro* testing, the disks were first constructed in CAD software, converted to STL format and then a slice file which was used to process the SCPC disks using the Z-Corp machine. Disks of size 10 mm diameter x 10 mm height were constructed for material characterization and disks of size 10 mm diameter x 2 mm height were processed to study the interaction of the SCPC with simulated body fluid (SBF). These disks were all processed using the Z-Corp machine in only minutes.

2.1.3 Effect of Thermal Treatment

SCPC disks were first thermally treated at a lower temperature to burn off the binder, and then sintered at a higher temperature to fuse the SCPC particles. In order to determine the thermal treatment required to burn off the hydrocarbons from the SCPC disks, several different temperatures were evaluated. SCPC disks (n=3) were treated at 300, 350, 400, or 450 ºC for 24 hours. If the hydrocarbons were not completely burned away the samples were left with a grayish color. The SCPC disks treated at 450 ºC were white after 24 hours of thermal treatment. Next, different thermal treatment durations were

Figure 2.1.2: Video of Z-Corp Processing

To begin building an implant the printer head sweeps across the feed and build boxes. The feed box rises supplying a thin layer of SCPC powder and the printer head pushes that across to the build box. Then the printer head sweeps across the build box, spraying a layer of the binder that is the same as the first cross-section of the part. The feed box will rise by one layer height and the build box will lower by one layer. The printer head will then push the next layer over to the build area creating the next layer. This process is then repeated over and over until the implant is created. The printer head will spray the binder, the feed box will raise, the build box will lower and the printer head will push the powder over creating the next layer. Excess powder is removed and the finished implant is removed from the Z-Corp. Any unused SCPC powder can then be recycled and used again.

evaluated in the same way. SCPC disks (n=3) were thermally treated at 450 ºC for 16, 18, 20 or 24 hours. It was found that treating the disks at 450 ºC for 18 hours sufficiently burned away all the hydrocarbons from the SCPC disks.

The effect of thermal treatment on the physicochemical properties of the SCPC material was then investigated for the sintering temperatures 800, 850, and 900 ºC. These treatment temperatures allowed for the formation of interconnectivity between the pores of the SCPC disks.

2.1.4 Material Characterization

2.1.4.1 Surface Characterization

To analyze the morphology of the SCPC disks, high resolution images were obtained by scanning electron microscope (SEM) operated at 20 kV acceleration voltage. First the disks were mounted on SEM stubs using colloidal graphite. The colloidal graphite was painted around the edges of the disks to facilitate electron conduction. The disks were then gold coated under an argon atmosphere using an Emscope SC400 sputter coater. This was done in order to facilitate electron conduction and assist the flow of electrons on the surface of the SCPC disks. The samples were then loaded into the microscope (Hitachi S-3200, Tokyo, Japan) and analyzed in the secondary image mode (SI).

2.1.4.2 Porosity Measurements

The porosity percent and specific surface area of SCPC disks processed using the Z-Corp machine and thermally treated at 800, 850, and 900 ºC were determined with the use of mercury intrusion and gas adsorption techniques (Micromeretics Co., Norcros, GA). The surface area of the samples was determined using the BET (Brunauer, Emmet, and Teller) theory. The thermally treated samples were cooled with liquid nitrogen and

analyzed by measuring the volume of gas (N_2) adsorbed at specific pressures. To measure the porosity percent and pore size distribution, mercury intrusion porosimetry was used. This technique involved placing the SCPC disks in a penetrometer, then surrounding the sample with mercury. Mercury was used because it is a non-wetting liquid to most materials and it resists entering voids or pores, doing so only when pressure is applied. The pressure applied to the mercury was increased from 0 psia to 60,000 psia. The pressure at which the mercury entered the pore was inversely proportional to the size of the pore.

2.1.4.3 Mechanical Properties

The compressive strength of the porous SCPC disks (10 mm diameter x 10 mm height) (n=5) which were subjected to various thermal treatments were evaluated using an Instron Machine Model 5582. The SCPC disks were loaded uniaxially at a rate of 0.005 in/sec until failure at room temperature. Load and displacement were measured continuously by the Instron testing machine and recorded. From this measured data, a stress-strain curve was derived and used to calculate ultimate compressive strength and failure strain of the SCPC disks. In addition, the values for the compressive modulus were derived from the stress-strain curves.

2.1.4.4 Evaluation of Release Kinetics of rhBMP-2

2.1.4.4.1 Recombinant Human BMP-2 Preparation

The recombinant human BMP-2 (rhBMP-2) used in this study was supplied by R&D Systems, Inc. (Minneapolis, MN). In order to reconstitute the 10 µg rhBMP-2 protein, 300 µL of 4 mM HCl containing 0.1% BSA (albumin bovine serum) was added to the protein, preparing a stock solution of 1 µg per 30 µL.

2.1.4.4.2 Release Kinetics of rhBMP-2

The SCPC implants (10 mm height x 5 mm width) (n=5) processed using the Z-Corp 3-D printer then thermally treated at 800, 850 or 900 ºC, and HA disks (10 mm diameter x 4 mm height) (n=5) were placed separately in a 24-well plate and sterilized by 100% ethanol for 30 min and then allowed to dry. Then the SCPC implants and HA disks were individually loaded with 30 µL of the reconstituted rhBMP-2. After the rhBMP-2 was evenly distributed on the ceramics, they were allowed to dry for 1 h. Next, each sample was individually placed in a snap cap vial and immersed in 10 mL of phosphate-buffered saline (PBS; pH 7.4) containing 1% BSA. All of the samples were placed in an incubator at 37 ºC for a period of 14 days. After various time periods, 1, 2, 4, and 12 hours, and 1, 2, 4, 6, 8, 10, 12 and 14 days, 2 mL of the existing immersion PBS solution were exchanged with 2 mL of fresh PBS solution. The concentration of BMP-2 released from the SCPC implants and the HA disks into the immersing solution was quantified with a Quantikine BMP-2 ELISA kit from R&D Systems, Inc. (Minneapolis, MN). The optical density of each well was determined using a microplate reader set to 450 nm. In order to account for wavelength correction, the optical density was also measured at 570 nm and subtracted from those readings done at 450 nm. From the rhBMP-2 standard dilutions supplied in the ELISA kit, the optical density versus the known concentration of the standards was plotted and a best-fit curve was drawn. The rhBMP-2 concentration of each sample could be determined by finding the absorbance value on the y-axis and using the best-fit curve, and then finding the corresponding rhBMP-2 concentration from the x-axis. Since after each time point the samples were diluted, the concentrations were multiplied by a dilution factor of 1.25 for each time point.

2.1.5 Study of the Interaction of SCPC with Simulated Body Fluid

2.1.5.1 Preparation of Simulated Body Fluid

In order to replicate that results that would occur *in-vivo*, the SCPC disks were immersed in simulated body fluid (SBF) (Table 2.1.5.1). According to Kokubo [39], this solution can precisely reproduce *in-vivo* surface structure changes, due to its similar ion concentration to human blood plasma.

2.1.5.2 Immersion Study

SCPC disks (10 mm diameter x 2 mm height), pre-treated at different temperatures, were placed in 6-well plates and immersed in 6 ml SBF for 12 hours, 1, 3, or 5 days. The plates were incubated at 37 ºC for the duration of the immersion time. At the end of each time period, the disks were removed from the SBF, rinsed with deionized water, dried at room temperature and used for surface analyses. The immersion SBF solution was dispensed into 15 ml centrifuge tubes and stored in a freezer for the analysis of SCPC dissolution kinetics.

2.1.5.3 SCPC Dissolution Kinetics

After immersion of the SCPC disks, the SBF ionic concentrations were analyzed by inductively coupled plasma-optical emission spectrometry (ICP-OES) (Perkin Elmer Optima 2000 DV, Wellesley, MA, USA). To analyze the concentrations of Ca, P, and Si, the collected SBF was diluted 3 times. To analyze the Na concentration, the SBF was diluted 36 times. These dilutions were necessary due to the ionic concentrations of the SBF being too high to be quantified by the machine. As a washing solution, 0.01% Triton X was prepared. Diluted SBF samples were placed in the autosampler tray along with the

Table 2.1.5.1: Simulated Body Fluid Concentrations

	Concentrations (mM)
Na^+	142.0
K^+	5.0
Mg^{2+}	1.5
Ca^{2+}	2.5
Cl^-	148.8
HCO_3^-	4.2
HPO_4^{2-}	1.0

standards of Ca, P, Si, and Na. The samples were then fed into the plasma. Atoms in the plasma emit photons with characteristic wavelengths for each element being analyzed. This photon emission is recorded by an optical spectrometer and when calibrated against the standards, this technique provided a quantitative analysis of the ionic concentrations of the SBF samples.

2.1.5.4 Surface Chemistry Analysis

To analyze modifications in the surface chemistry during immersion in SBF, the functional groups on the surface of the SCPC disks, before and after immersion in SBF, were analyzed by Fourier Transform Infrared Spectroscopy (FTIR) (Thermo Nicolet Nexus 670 FT-IR, Madison, WI, USA). The disks were analyzed in the diffuse reflectance mode in the wave number range of 400–4000 cm^{-1}. The spectra of the immersed SCPC disks were compared to the spectra of SCPC before immersion in SBF. A spectrum for KBr was used as a background.

2.1.5.5 Surface Modification

To analyze the morphology of the SCPC disks after immersion in SBF, images were obtained by SEM as previously described.

2.2 *In-Vivo* Study

2.2.1 Experimental Setup

2.2.1.1 General Experimental Protocol

Nine male New Zealand White Rabbits (3 kg, Myrtle's Rabbitry, Thompson Station, TN, USA) were used to evaluate tissue response to the SCPC implant. The rabbit ulna was subjected to CT scan and the CT file was used with a Z-Corp machine to make a bone prototype employing SCPC powder. To induce osteoinduction, the SCPC implant was loaded with 10 µg of rhBMP-2. rhBMP-2 was used because of its significant role in inducing bone cell differentiation, which is well documented in the literature [1, 2, 7-9, 23, 24]. Surgical procedures were performed to remove a 10 mm segment of the ulna and then the defect was grafted with the SCPC-rhBMP-2 hybrid. Plates and screws were used to provide initial fixation. After 12 or 16 weeks the animals were euthanized. The morphology and mechanical strength of the regenerated bone were analyzed.

2.2.1.2 Prototype Processing

Prior to surgery, the rabbits had CT scans (Siemens Somatom Plus 4, Siemens Somatom Sensation 10, Erlangen, Germany) performed on their right forearms. For the CT scans the rabbits were anesthetized with 10 mg/kg xylazine subcutaneously and 50 mg/kg ketamine intramuscularly. The CT data was then converted into STL format, which remapped the surface data to a series of triangles. These images were then imported into the Amira CAD software where adjustments could be made (Figures 2.2.1.2 (a-b)). Using the CAD software, the ulna was isolated from the radius. Then a 10 mm bone segment was removed in the image; 20 mm proximal to the styloid process (Figure 2.2.1.2 (c-e)). The final CAD image of the defect was then converted back into a STL

Figure 2.2.1.2 (a-e): Z-Corp Processing

These images are of the CT scan data that has been converted into a CAD file. Figure 2.2.1.2 (a) shows the rabbit legs as they would normally appear.

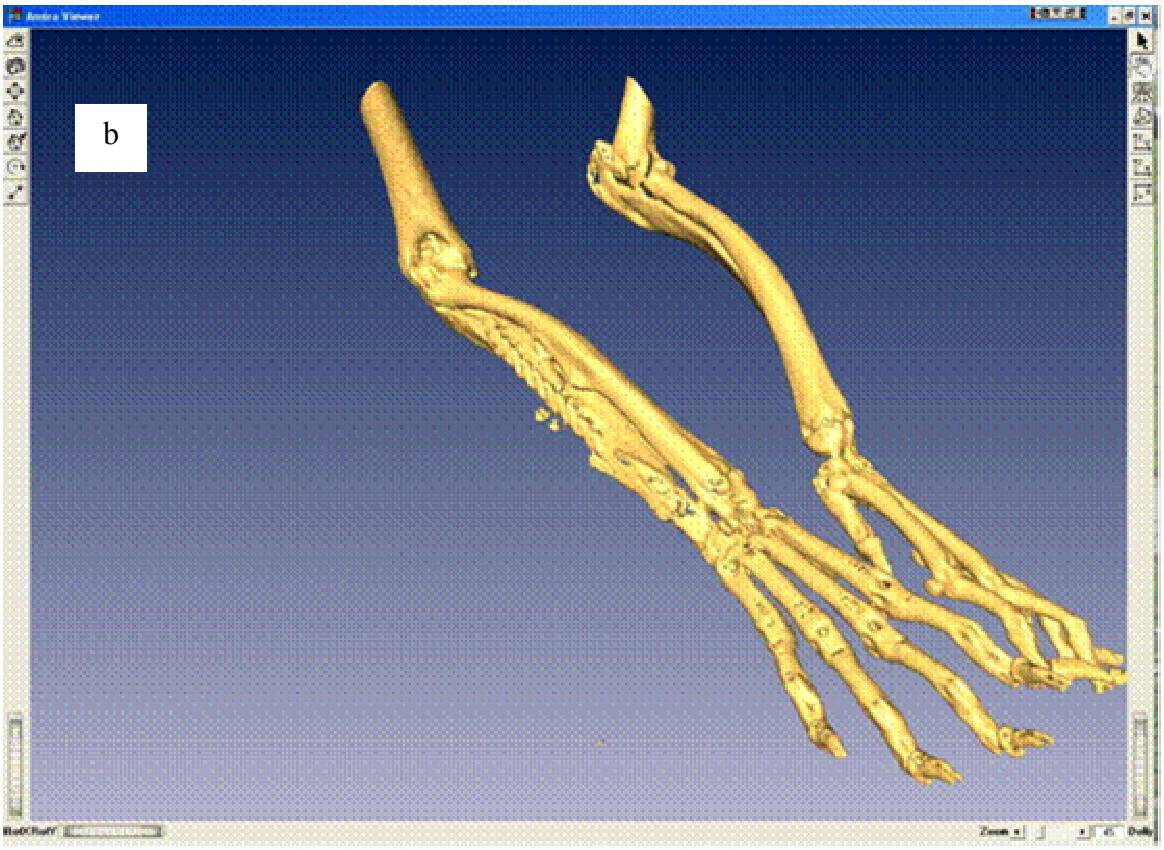

Figure 2.2.1.2 (a-e): Z-Corp Processing (continued)

These images are of the CT scan data that has been converted into a CAD file. Figure 2.2.1.2 (b) shows the same image as Figure 2.2.1.2 (a) but with the outer layers removed so that only the bones can be seen. All of this is done using Amira CAD software. From here the ulna can be isolated.

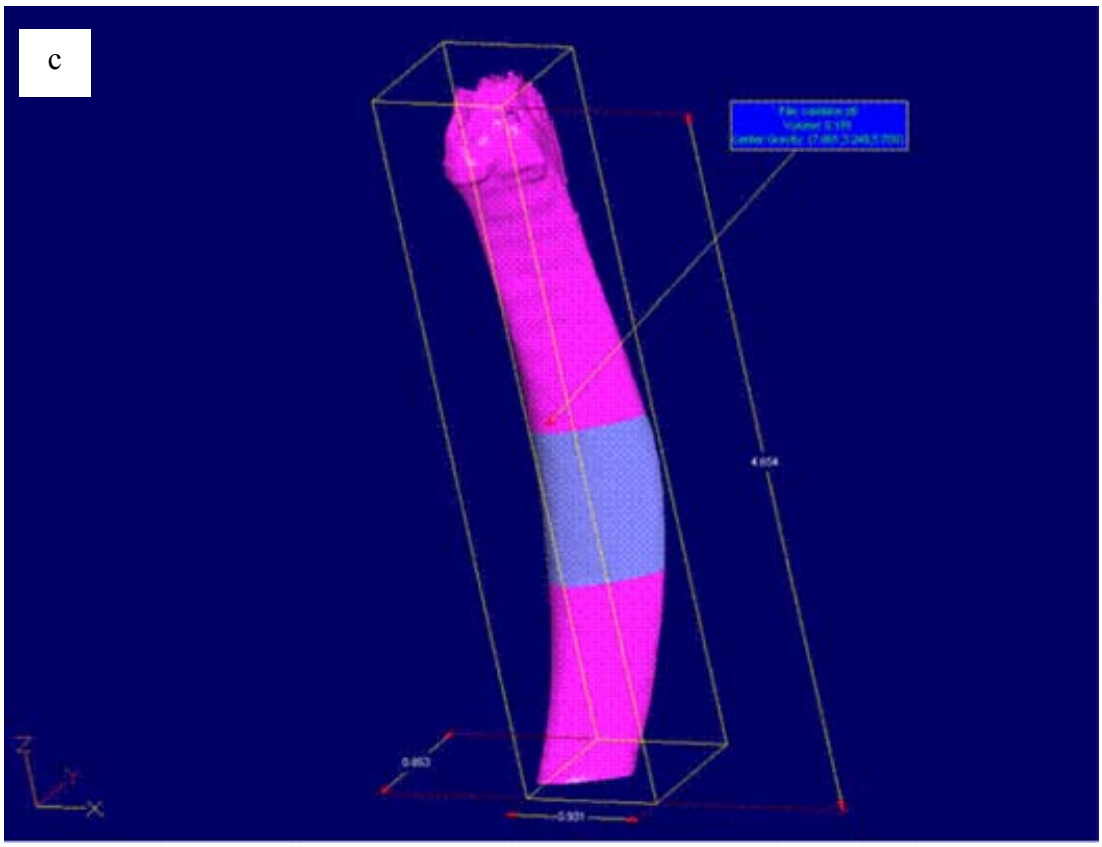

Figure 2.2.1.2 (a-e): Z-Corp Processing (continued)

These images show the isolated ulna in the CAD software. Figure 2.2.1.2 (c) shows the 10 mm segment to be sectioned out of the ulna 20 mm proximal to the styloid process.

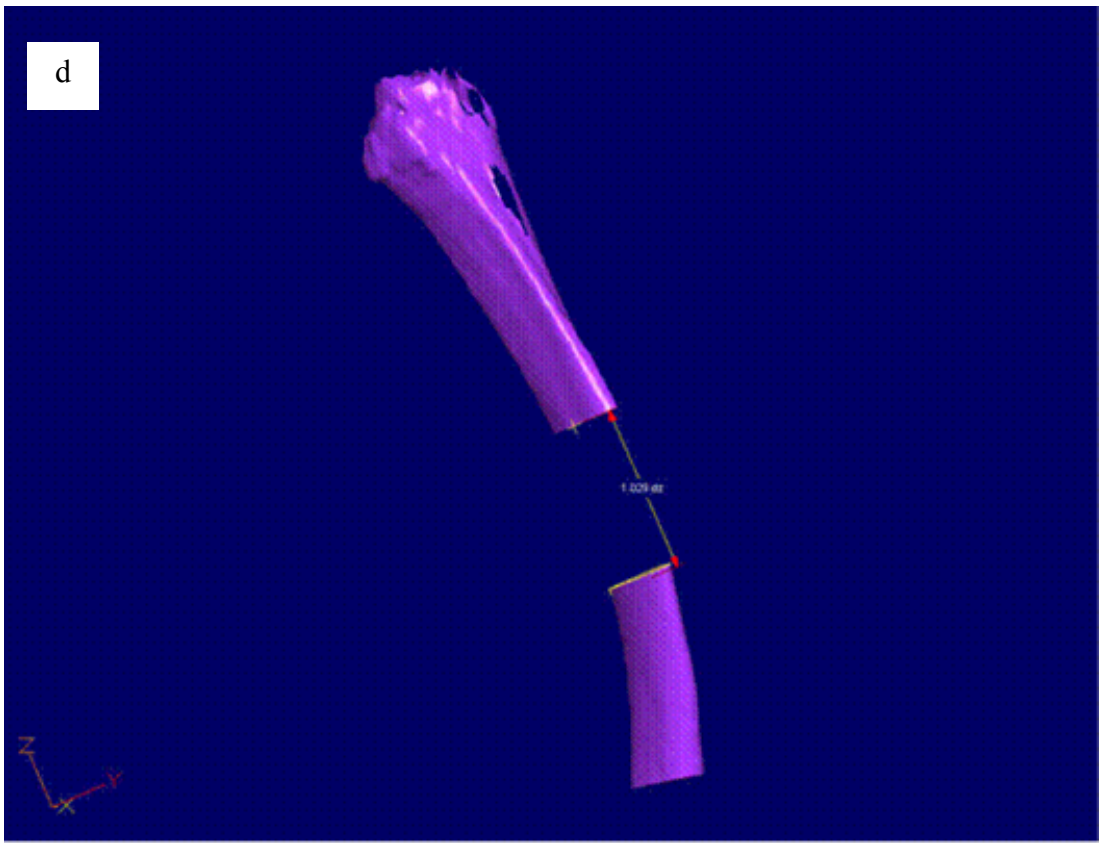

Figure 2.2.1.2 (a-e): Z-Corp Processing (continued)

These images show the isolated ulna in the CAD software. Figure 2.2.1.2 (d) shows the ulna with the segment removed.

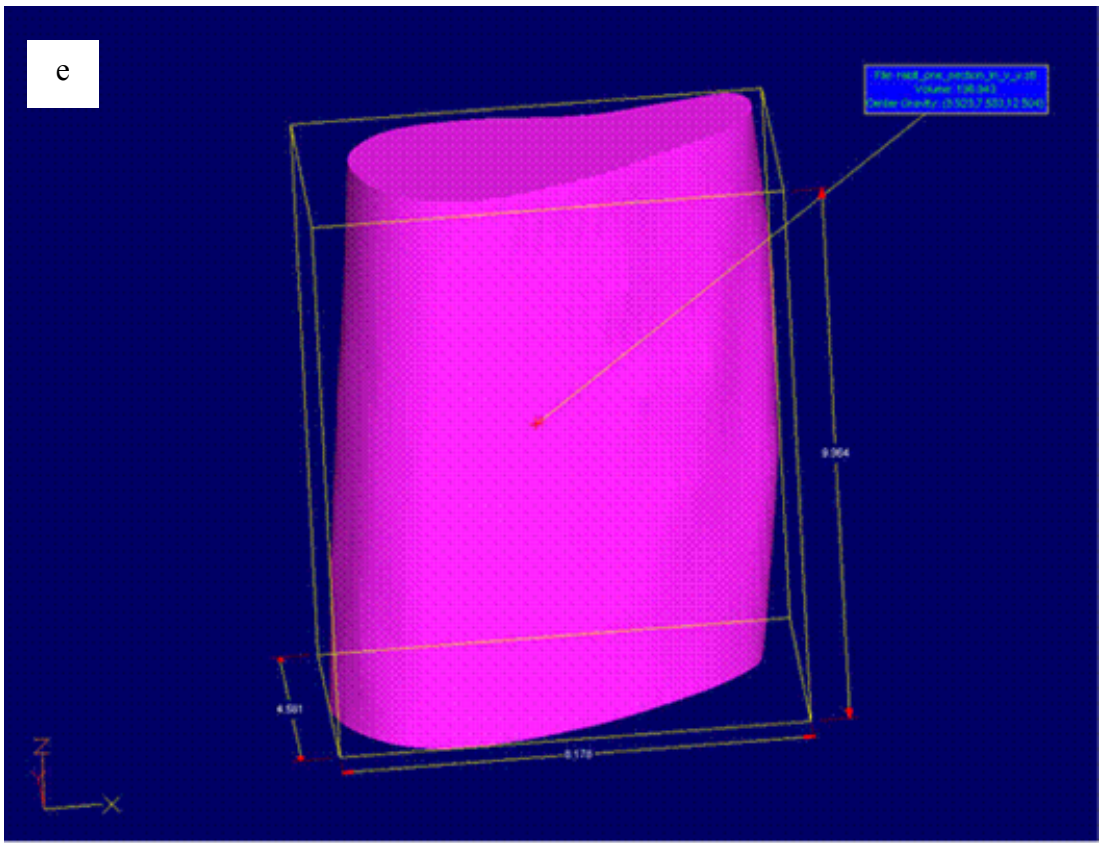

Figure 2.2.1.2 (a-e): Z-Corp Processing (continued)

These images show the isolated ulna in the CAD software. Figure 2.2.1.2 (e) is an enlarged image of the 10 mm segmental defect to be replicated using the SCPC powder and fabricated using the Z-Corp processing RP technique. It can be seen that the geometry and topography of the defect is complicated.

format, and then into a slice file that the Z-Corp machine used to replicate the removed bone segment layer by layer. To synthesize the desired implant, the Z-Corp spread out a thin layer of the SCPC powder, then the ink-jet printer head printed a water-based binder in the cross-section of the implant being created. The build piston which had the SCPC powder then would drop down, making room for the next layer, and the process was repeated until an implant that exactly replicated the removed bone segment had been processed.

2.2.1.3 Thermal Treatment

The implants processed by the Z-Corp were heat treated at 450 ºC for 18 hours to burn off the binder used to secure the layers and any other hydrocarbons and then at 800, 850 or 900 ºC for 3 hours to sinter the SCPC implants.

2.2.1.4 Sterilization

Prior to surgery, the implants were sterilized by immersing them in 70% ethanol for 30 minutes under a sterile hood. Tweezers, used for handling the implants, were also immersed in ethanol. After sterilization, the implants were placed in sterile cell culture dishes to dry.

2.2.1.5 Construct of SCPC-rhBMP-2 Scaffold

In order to reconstitute the rhBMP-2, 40 µl of 4mM HCl containing 0.1% BSA was sterilized by filtering through a 45 µm pore opening and then dispensed into a vial containing 10 µg of rhBMP-2. The BSA was added to prevent loss in activity caused by non-specific binding of BMP to the inside surface of the vial. The BMP solution was immediately dispensed evenly on all sides of the sterilized SCPC implant.

2.2.1.6 Surgery

Rabbits were anesthetized with an intravenous injection of 10 mg/kg xylazine followed by 50 mg/kg ketamine. The right forearm was shaved and the skin was sterilized with povidone-iodine and draped with sterile towels. Under aseptic conditions, the right ulna was exposed through a straight incision of approximately 3 cm long. The ulna was separated from the surrounding muscles and the periosteum was cut through to expose the ulna bone. A critical sized segmental defect was then created in the ulna of the right forelimb by removing 10 mm of midshaft diaphyseal bone 20 mm proximal to the styloid process.

The SCPC implant, thermal treated at 800 (n=1), 850 (n=2) or 900 ºC (n=6), was placed in the defect. The implant, made individually for each rabbit using the Z-Corp machine, was secured in place using plate and screws. Using Vicryl, the incision was closed subcutaneously layer by layer, to prevent the rabbit from chewing out any sutures. Then skin glue was placed over the outside of the incision. The rabbits received 0.05 mg/kg buprenorphine 30 minutes prior to the end of surgery and then every 8 to 12 hours as needed for pain. After recovery, the rabbits were allowed to be load bearing without external support on the leg.

Two rabbits died prior to surgery, during anesthetizing, due to unknown complications. These rabbits were to have received SCPC implants thermally treated at 850 ºC.

2.2.2 Evaluation of SCPC-rhBMP-2 Graft

2.2.2.1 Radiographic Evaluation

In order to evaluate bone formation, union and remodeling of the defect, CT scans were performed postoperatively at 4, 8, and 12 weeks. The CT scans were performed at 64

slices per rotation with an isotrope CT resolution of 0.4 mm. The high resolution CT data was then converted into STL data format, remapping the surface data into a series of triangles, and then imported into a CAD file. This allowed for a non-invasive 3-D view of the remodeled defect.

2.2.2.2 Histology

The ulna treated with an 800 ºC thermally treated SCPC-rhBMP-2 hybrid implant was harvested from a rabbit that was euthanized by an overdose of sodium pentobarbital 16 weeks post-operatively. This ulna was used for non-decalcified histological evaluation. The bone specimen was fixed in 10% buffered formalin solution and then embedded in polyethlymethacrylate (PMMA), and the non-decalcified sections (40 μm) were ground and prepared using an Exakt machine (Exakt Technologies, Inc., Oklahoma City, OK). The sections were made along the long axis of the ulna and were stained with Toluidine Blue and examined for histological evaluation.

2.2.2.3 Torsional Testing

In order to assess the mechanical properties of the rabbit ulna, the ulna was subjected to torsional testing. Each rabbit treated with a 900 ºC thermally treated SCPC-rhBMP-2 hybrid implant was euthanized at 12 weeks postoperatively. Both ulnae (grafted (n=3) and ungrafted (n=3)) from each rabbit were harvested, cleaned of soft tissue and used for mechanical testing. Specimens with insufficient bone healing (n=3), due to failure of the fixation device, were excluded from torsional testing. The fixation devices on those ulnae with sufficient healing were carefully removed. Care was taken to ensure that no excessive mechanical loads were applied to these ulnae during the harvesting process. Each harvested ulna was then immediately wrapped in gauze moistened with Ringers solution, sealed in a labeled storage bag, and then fresh frozen at -20 ºC until testing.

All ulnae to be mechanically tested were defrosted by removing them from the freezer and storing them in a refrigerator at 2 °C for 24 hours prior to testing, while still wrapped with gauze moistened with Ringers solution. Then the ulnae were removed from the sealed storage bag and prepared for testing by trimming the grafted ulna with a slow speed diamond wafer saw blade subjected to constant irrigation at sites 2 cm proximal and distal from the proximal and distal defect ends, so that the total length of the testing sample was 5 cm. The ungrafted ulna was also isolated and trimmed at the corresponding sites so it too had a length of 5 cm.

Once the ulnae were at the appropriate length, both ends of the bone were inserted into a custom-made alignment fixture, and 1 cm of each end of the ulna was potted in JB Weld. This custom made alignment fixture was used to ensure that the longitudinal axis of the bone was parallel and concentric with the torsional testing axis. It also ensured that the gauge length (the total length of the ulna unpotted) was consistent to ±1 mm, and this amount was measured by using a pair of digital outside vernier calipers accurate to 0.01 mm. During the healing of the bone defect, bony fusion had occurred between the ulna and the radius. Separation of the radius from the ulna was not possible due to the fibrous fusion. All limbs were kept physiologically moist by keeping the gauze moistened with Ringers solution continually wrapped around the ulnae throughout the potting and testing procedures.

After approximately 24 hours of room temperature hardening, the potted specimens were mounted in a custom built torsional testing fixture which was secured to a computer-controlled, biaxial servo-hydraulic material testing system (Instron 8521, Canton, MA, USA). Mechanical testing to failure was performed at room temperature. With the proximal end held fixed, the distal end was externally rotated at a constant rate of 90 $°min^{-1}$ until failure. For those specimens with no clear failure, the maximum rotation and energy to failure was computed for a displacement up to 35 °. Torque versus angular deformation curves were obtained by using the accompanying Instron System 8800 Controller. Maximum torsional load to failure and angle at failure were measured.

After the specimens had catastrophically failed, the cross-sectional areas of the ulnae were obtained by sectioning with a diamond wafer saw blade subjected to continuous irrigation. These cross-sections were photographed, and the cross-sectional areas were calculated by using image analysis freeware (NIH Image 1.59, Bethesda, MD, USA). The calculated cross-sectional area data, along with the gauge length and other measured torsional test data were then used to calculate the values of maximum torsional load to failure and torsional angle at failure for grafted and control ungrafted bone. All broken torsional testing specimens were properly labeled with an indelible ink marker and returned to their marked storage bags, and then refrozen in the event that additional study was needed.

2.3 Statistical Analysis

Representative values of parameters used in this study were shown as mean ± standard deviation. Each parameter was statistically analyzed by a t-test with two samples assuming unequal variances. A *p*-value of less than 0.05 was considered to be statistically significant.

Chapter 3

Results

3.1 Material Characterization

3.1.1 Morphology Analysis

SEM of the SCPC disks processed using the Z-Corp machine and thermally treated at 800, 850, and 900 ºC showed the disks to be highly porous with interconnected pathways between the pores (Figure 3.1.1 (a-d)). For all thermal treatment temperatures at high magnification, a porous structure containing micropores of size range 20-100µm is visible and the interconnections between these pores are in the range of 10 - 50 µm. Figure 3.1.1 (a) shows two large micropores that are surrounded by interconnected pathways in a disk treated at 800 ºC. Figure 3.1.1 (b) shows that the disk treated at 850 ºC has a similar structure of micropores and interconnections. Figure 4.1.1 (c) shows that pores on the SCPC disk thermally treated at 900 ºC has smoother edges and are more defined. The micrographs show that as the thermal treatment temperature of the SCPC disks is increased the particle edges become smoother showing a greater level of interconnectivity between the pores. Moreover, at a higher magnification, it can be seen that the surface of the SCPC disks are covered by nanopores (Figure 3.1.1 (d)).

3.1.2 Porosity Measurements

Table 3.1.2 summarizes the results from the porosity and surface area analysis. The analysis of the porosity shows that the porosity is greatest for the SCPC disks thermally treated at 800 ºC with a porosity percent of 54%, then 50% at 850 ºC, and then 900 ºC had the porosity percent of 44%. The surface area of the thermally treated SCPC disks also was greatest for the lower sintering temperature. The disks treated at 800 ºC had a

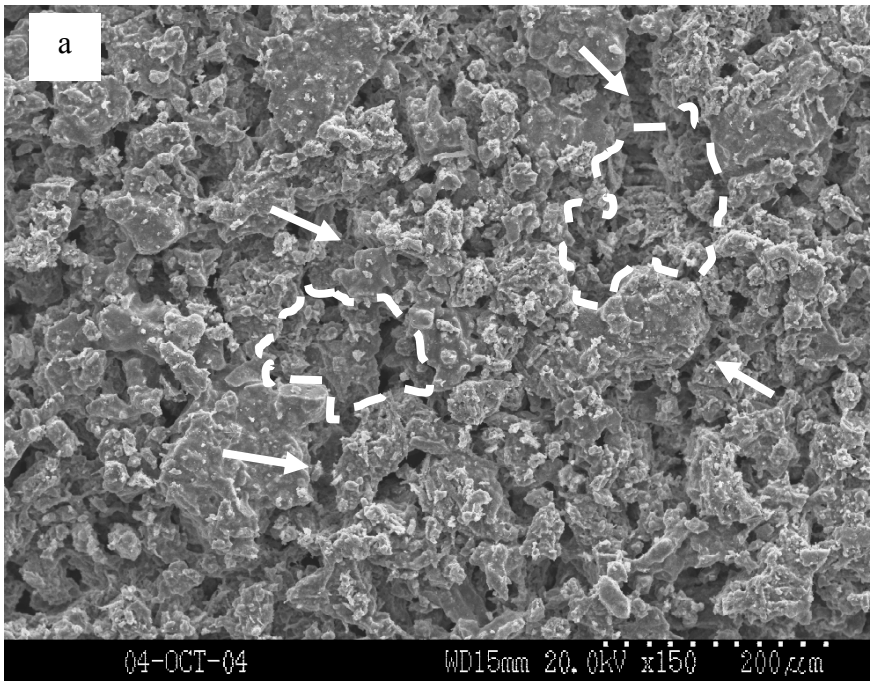

Figure 3.1.1 (a-d): SEM Micrographs Before Immersion

SEM micrographs of SCPC disks show that the particle edges become smoother as the thermal treatment temperature is increased. (a) Two large micropores (dashed lines) of the disks treated at 800 ºC are surrounded by interconnected pathways of smaller pores (arrows).

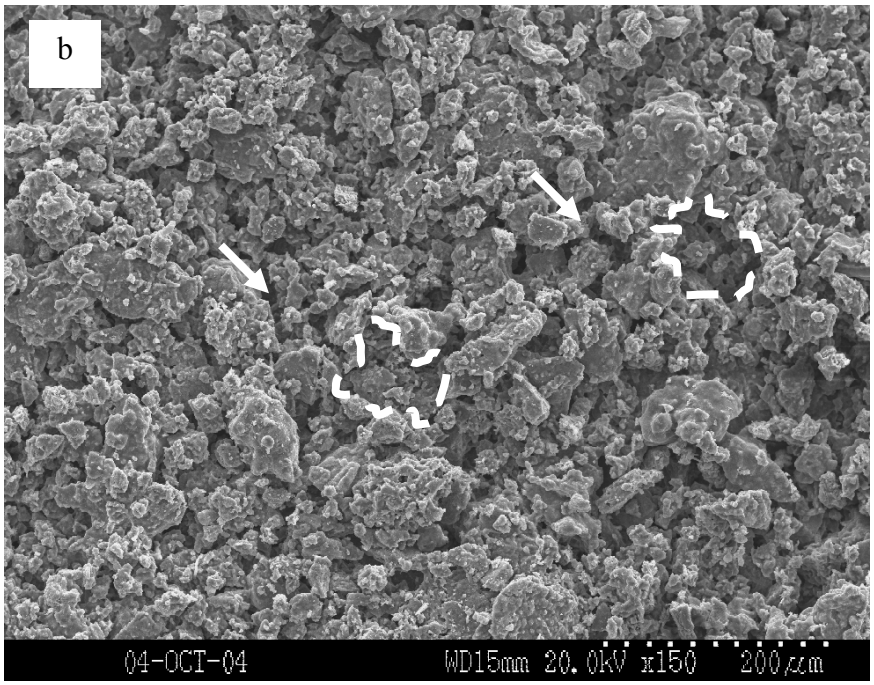

Figure 3.1.1 (a-d): SEM Micrographs Before Immersion (continued)

SEM micrographs of SCPC disks show that the particle edges become smoother as the thermal treatment temperature is increased. (b) Disks treated at 850 ºC show a similar structure of micropores (dashed lines) and smaller interconnected pores (arrows).

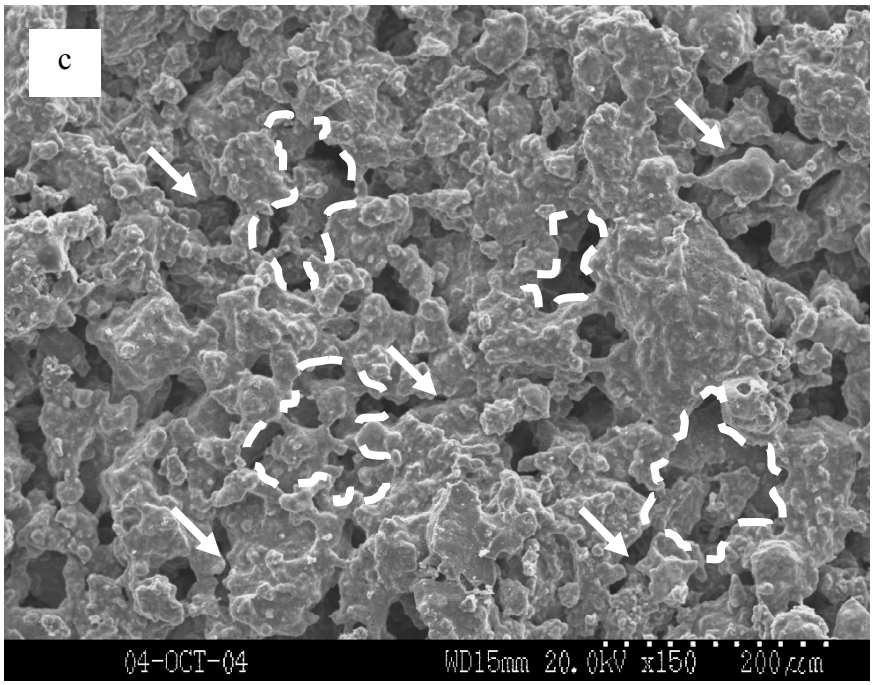

Figure 3.1.1 (a-d): SEM Micrographs Before Immersion (continued)

SEM micrographs of SCPC disks show that the particle edges become smoother as the thermal treatment temperature is increased. (c) Disks treated at 900 ºC show more defined micropores (dashed lines) and interconnection (arrows) with smoother edges.

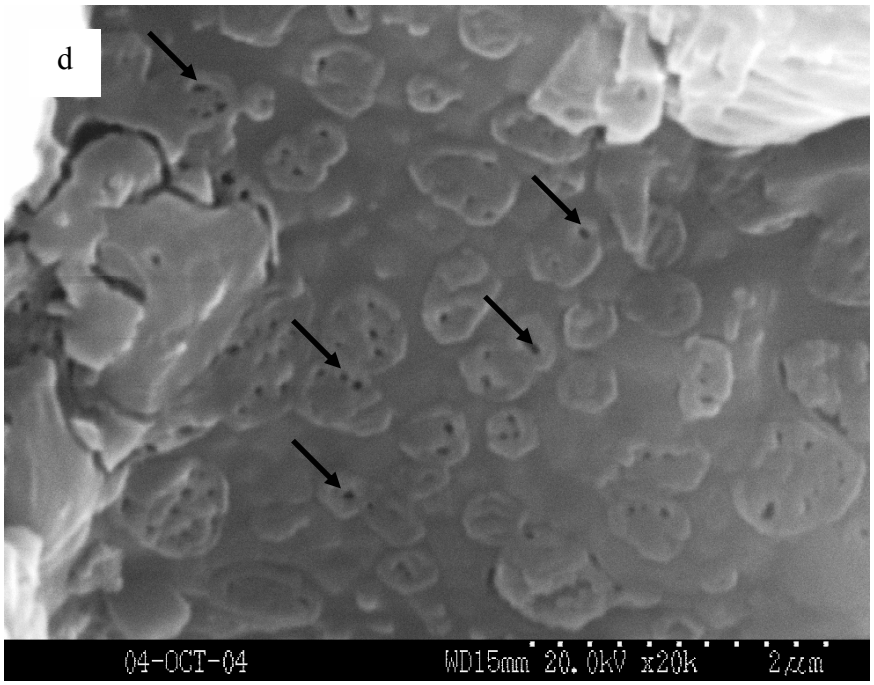

Figure 3.1.1 (a-d): SEM Micrographs Before Immersion (continued)

SEM micrographs of SCPC disks show that the particle edges become smoother as the thermal treatment temperature is increased. (d) High magnification of the disks treated at 850 ºC reveal that the disks are not only microporous, but the surface is also covered with nanopores (arrows), providing for a large surface area for drug delivery.

Table 3.1.2: Porosity Analysis

Porosity analysis shows that the porosity percent and surface area were dependent on the thermal treatment of the SCPC disks. As the thermal treatment temperature was increased the porosity percent and surface area both decreased.

Treatment Temperature	Pore Size Distribution %					As determined by BET and Hg intrusion	
	356-100 µm	100-25 µm	25-10 µm	10-1 µm	1 µm-4 nm	Surface Area (m^2/g)	Porosity %
800 ºC	3.00	22.86	48.76	22.42	2.96	3.442	54
850 ºC	2.71	7.12	70.71	17.88	1.57	2.814	50
900 ºC	4.74	12.73	60.36	19.69	2.48	2.615	44

surface area of 3.442 m^2/g, then 2.814 m^2/g at 850 ºC, and those treated at 900 ºC had a surface area of 2.615 m^2/g. As for the pore size distribution, the thermal treatment temperature had no effect on the distribution of pores greater than 100 µm or less than 10 µm. However, for the SCPC disks treated at 800 ºC, 48.76% of the pores were in the range of 25 µm-10 µm while 22.86% were in the range of 100 µm-25 µm. When the thermal treatment was changed to 850 ºC, the percent of pores in the range of 25 µm-10 µm jumped up to 70.71% and the percent dropped to 7.12% in the 100 µm-25 µm range. For the disks treated at 900 ºC, the percent of pores in the range of 25 µm-10 µm decreased down to 60.36% and the percent of pores in the range of 100 µm-25 µm increased to 12.73%.

3.1.3 Mechanical Testing

The mechanical properties of the SCPC disks were dependent on the thermal treatment temperature (Table 3.1.3). The compressive strengths and modulus of the disks significantly increase with the increase of the thermal treatment temperature (n=5, $p<0.04$). The ultimate compressive strength and the compressive modulus of the disks range from 5-15 MPa and 300 MPa-1.1 GPa, respectively. The disks treated at 900 ºC have a significantly higher compressive strength and modulus as compared to those disks treated at 800 ºC ($p<0.003$) and 850 ºC ($p<0.003$). Moreover, the disks treated at 850 ºC have a significantly higher compressive strength and compressive modulus as compared to the disks treated at 800 ºC, $p<0.008$ and $p<0.0006$, respectively. These results are consistent with the SEM results showing that as the thermal treatment temperature increased, there is greater interconnectivity between the SCPC particles, and thus greater mechanical strength. Conversely, as the porosity percent of the SCPC disks is increased the mechanical strengths decrease.

Table 3.1.3: Mechanical Properties Results

Mechanical properties of the SCPC disks after thermal treatment indicate that the ultimate compressive strength and the compressive modulus of the disks increased as the thermal treatment temperature increased. The ultimate compressive strength of the disks (5-15 MPa) is comparable to that of trabecular bone (2-12 MPa). However, as the porosity percent increased (Table 3.1.2) the mechanical strength decreased.

Treatment Temperature	Ultimate Compressive Strength	Failure Strain	Compressive Modulus
800 ºC	5.584 ± 0.52 MPa	0.0198 ± 0.003	307 ± 44MPa
850 ºC	8.977 ± 1.60 MPa	0.0164 ± 0.002	551± 56 MPa
900 ºC	15.326 ± 2.95 MPa	0.0138 ± 0.005	1095 ± 164 MPa

3.1.4 Release Kinetics of rhBMP-2

Analysis of the release kinetics of rhBMP-2 from the SCPC-rhBMP-2 hybrid and the HA-rhBMP-2 hybrid showed that after 2 days the concentration of rhBMP-2 released was not significantly different between the two (Figure 3.1.4). However, after 2 days, the amount of rhBMP-2 released from the SCPC-rhBMP-2 hybrid is significantly greater (p<0.04), than that of the HA-rhBMP-2 hybrid. At 14 days the concentrations of rhBMP-2 is not significantly different between the two hybrids.

3.2 Interaction of SCPC with SBF

3.2.1 ICP

ICP analyses of the ionic concentrations of SBF for calcium (Ca), phosphorus (P), silicon (Si) and sodium (Na) after immersing thermally treated SCPC disks in the SBF are shown in Figure 3.2.1 (a-d). Analysis shows that the Ca concentration of the SBF incubated with all SCPC disks drops drastically after the first 12 hours of immersion (Figure 3.2.1 (a)). Moreover, thermal treatment has a profound effect on the corrosion behavior of the material. The Ca concentration of SBF incubated with SCPC treated at 800 ºC is significantly (n=3, p<0.03) higher than the Ca concentration of SBF incubated with SCPC treated at 850 and 900 ºC. However, the difference in Ca concentration of the SBF incubated with SCPC treated at 850 or 900 ºC is not significantly different. After 12 hours, the Ca concentration of the SBF decreases according to the temperature of the treatment of the ceramic in the order 800 ºC > 850 ºC > 900 ºC. Similar concentrations of Ca are measured in the immersion solution after 12 hours, and 1, 3, and 5 days for all disks which indicates equilibrium between the dissolution and precipitation reactions at the material-solution interface.

In contrary to the immediate decrease in the Ca concentration, the P concentration significantly increases after the first 12 hours and then after 1 day begins to slope down

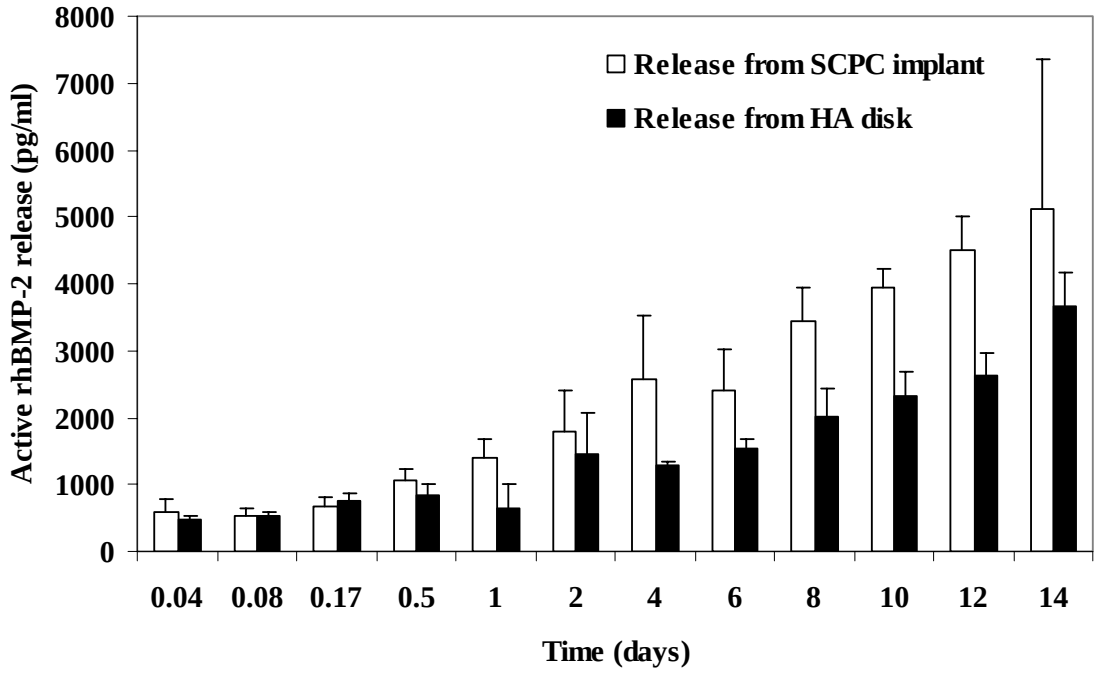

Figure 3.1.4: Cumulative Release of rhBMP-2 from SCPC and HA

The graph of the cumulative release of rhBMP-2 from the SCPC implant and the HA disk shows that the release from the SCPC implant is greater than that from the HA disk. This release was significantly more (p<0.04) from 4-12 days.

a

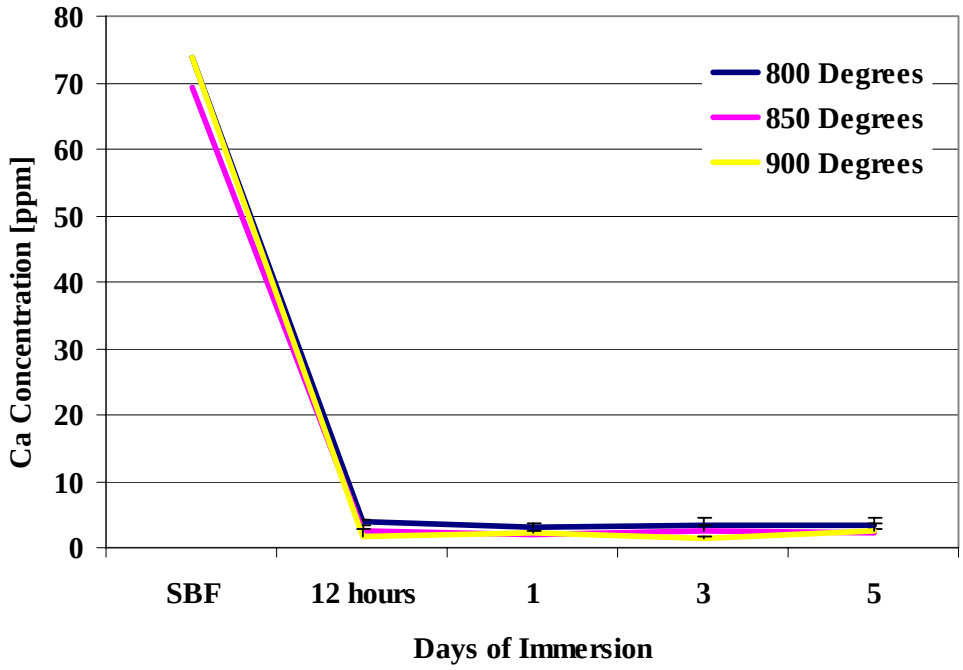

Figure 3.2.1 (a-d): ICP Results

ICP results show the ionic concentrations of SBF incubated at 37 ºC with thermally treated SCPC disks. (a) The Ca concentration of SBF decreased due to the precipitation of a HA layer onto the SCPC surface.

b

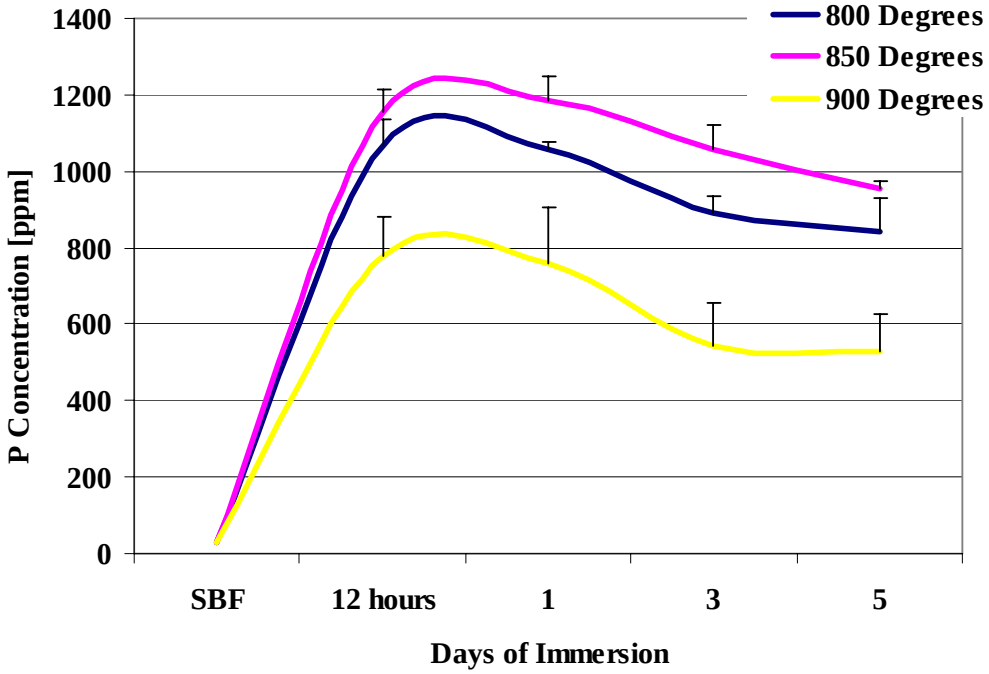

Figure 3.2.1 (a-d): ICP Results (continued)

ICP results show the ionic concentrations of SBF incubated at 37 ºC with thermally treated SCPC disks. (b) In contrary to the Ca decrease, the P concentration of SBF increased due to not all P ions dissolving from the material being consumed in the formation of a HA surface layer.

c

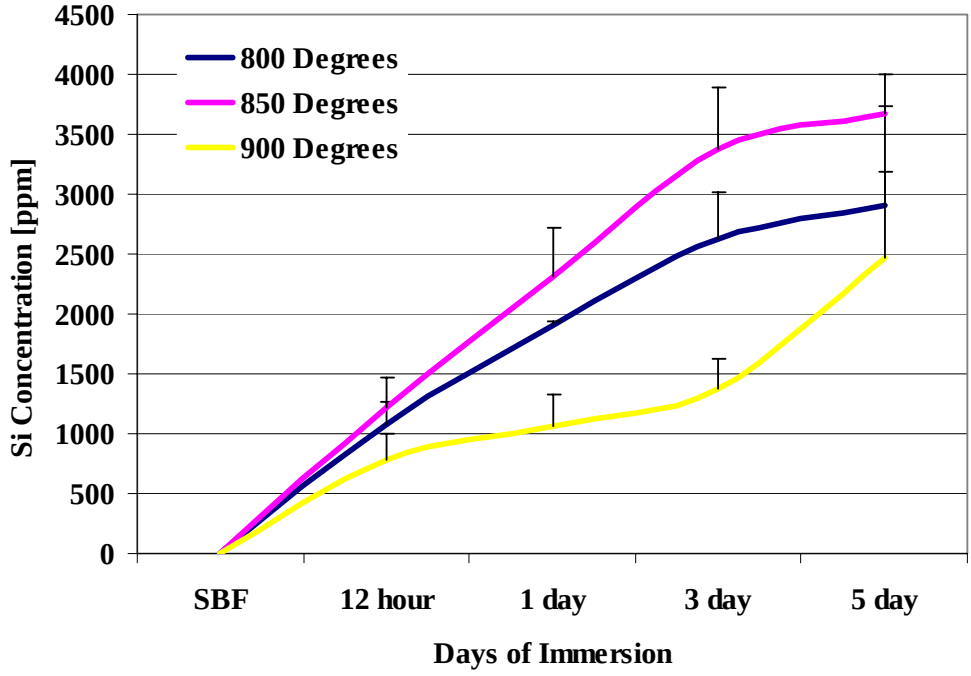

Figure 3.2.1 (a-d): ICP Results (continued)

ICP results show the ionic concentrations of SBF incubated at 37 ºC with thermally treated SCPC disks. (c) The Si concentration increased as the immersion time increased. This was due to its dissolution from the SCPC disk into the SBF, allowing for the nucleation of a HA layer apart form the SCPC disk.

d

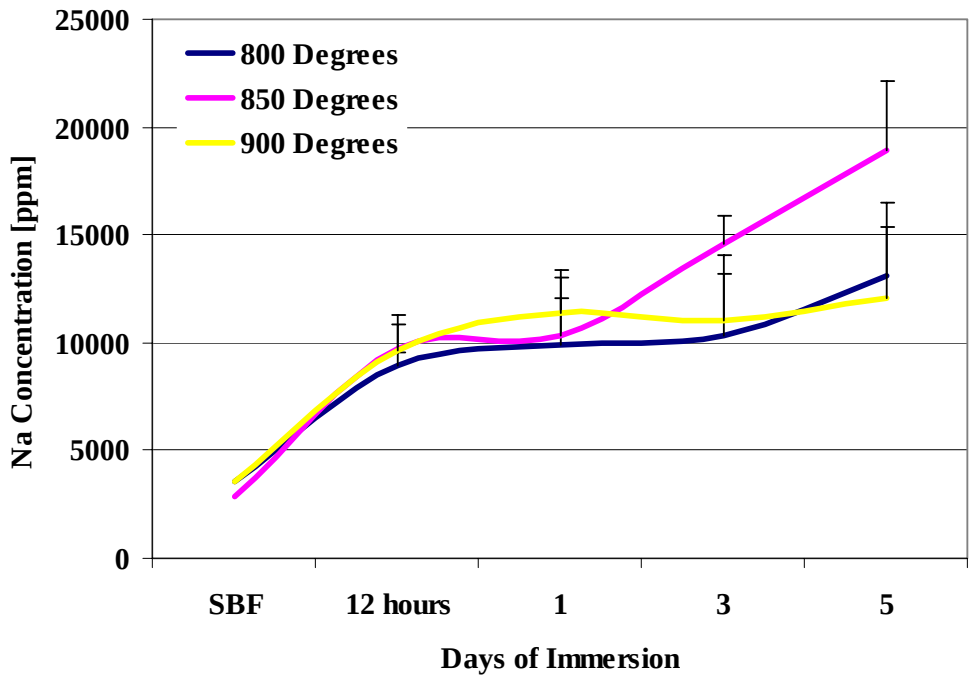

Figure 3.2.1 (a-d): ICP Results (continued)

ICP results show the ionic concentrations of SBF incubated at 37 ºC with thermally treated SCPC disks. (d) The Na concentration of the SBF increased as the immersion time increased. As the SCPC disk was immersed, there was dissolution of Na from the SCPC into the SBF.

and plateau out (Figure 3.2.1 (b)). The ICP results also show that the thermal treatment temperature has a significant effect on the corrosion of P. After 12 hours of immersion, the P concentration of the SBF decreases according to the thermal treatment temperature of the ceramic in the order 850 ºC > 800 ºC > 900 ºC. The SBF incubated with SCPC disks thermally treated at 850 ºC has a significantly higher (n=3, $p<0.02$) P concentration than the P concentration of SBF incubated with SCPC treated at 850 ºC, which is in turn significantly higher (n=3, $p<0.01$) than the P concentration of SBF incubated with SCPC treated at 900 ºC. Even with these significant differences, they all follow the same trend of significantly increasing after the first 12 hours and then after 1 day through the rest of the immersion time begin to plateau out. This plateau shows that the P concentrations of the SBF are reaching the equilibrium state in the same way that the Ca concentrations are, and for the same reason.

The Si concentration of the SBF exhibits a significant linear increase for the duration of the immersion times (Figure 3.2.1 (c)). After all immersion times, the Si concentration of the SBF incubated with SCPC disks shows that the thermal treatment has a major impact on the corrosion behavior of the SCPC disks. The Si corrosion increased according to the thermal treatment temperature of the ceramic before immersion in the order 850 ºC > 800 ºC > 900 ºC. The SBF incubated with SCPC disks thermally treated at 850 ºC has a significantly higher (n=3, $p<0.03$) Si concentration than the Si concentration of SBF incubated with SCPC treated at 800 ºC, which in turn is also significantly higher (n=3, $p<0.03$) than the Si concentration of SBF incubated with SCPC treated at 900 ºC. Nevertheless, even with these significant differences, they all follow the trend of increasing linearly through 3 days of immersion. After 3 days, the Si concentration of the SBF incubated with SCPC thermally treated at 800 and 850 ºC begins to show signs of leveling off. Conversely, the Si concentration of the SBF incubated with SCPC treated at 900 ºC continues to increase.

The concentration of Na of the SBF also increases gradually as the immersion duration progresses (Figure 3.2.1 (d)). For the Na concentrations, the thermal treatment temperature of the SCPC disks has little effect on their corrosion, showing no significant

differences in the concentrations. The Na concentration of the SBF incubated with the thermally treated SCPC disks increases from the initial concentration to 12 hours of immersion and then begins to plateau out after 12 hours of immersion. The concentration of the SBF incubated with the disks treated at 800 and 900 ºC continues to level off after 3 days of immersion and then begins to increase again. The Na concentration of the SBF incubated with the disks treated at 850 ºC also begins to level off after 12 hours of immersion, but unlike the other thermal treatment temperatures, begins to increase again after 1 day of immersion. Even so, these differences are no statically significant, so the thermal treatment of the SCPC disks does not affect the Na concentration of the SBF that they are immersed in.

3.2.2 FTIR

Prior to immersing the SCPC disks in SBF, FTIR spectra of the SCPC surface at all thermal treatment temperatures demonstrate similar function groups, including distinct Si signals (Figure 3.2.2 (a-c)). These signals include the Si─O bending mode at 520 cm^{-1} and S─O vibrational stretch at 1098 cm^{-1}. The peak at 848 cm^{-1} is a result of the P─OH stretching mode of HPO_4. Peaks that are characteristic for the bending vibrational modes of P─O are demonstrated at 568, 611, and 1052 cm^{-1}. The shoulder peak at 925 cm^{-1} is due to Si ─O^{-+}Na bonds that occur in the SCPC composite.

After 12 hours of immersion in SBF, FTIR spectra for the different thermal treatment temperatures of SCPC disks demonstrate altered surface functional groups. The immersion in SBF causes the development of a new peak for C─O vibrational mode of carbonate at 860 cm^{-1}. Peaks for P─O, characteristic of carbonate hydroxyapatite, are observed at 565, 605, and 1035 cm^{-1}. As the presence of new peaks demonstrates the formation of a hydroxyapatite layer on the surface of the SCPC disks, the peaks characteristic for Si─O^{-+}Na and Si─O vibrational stretch become less prominent.

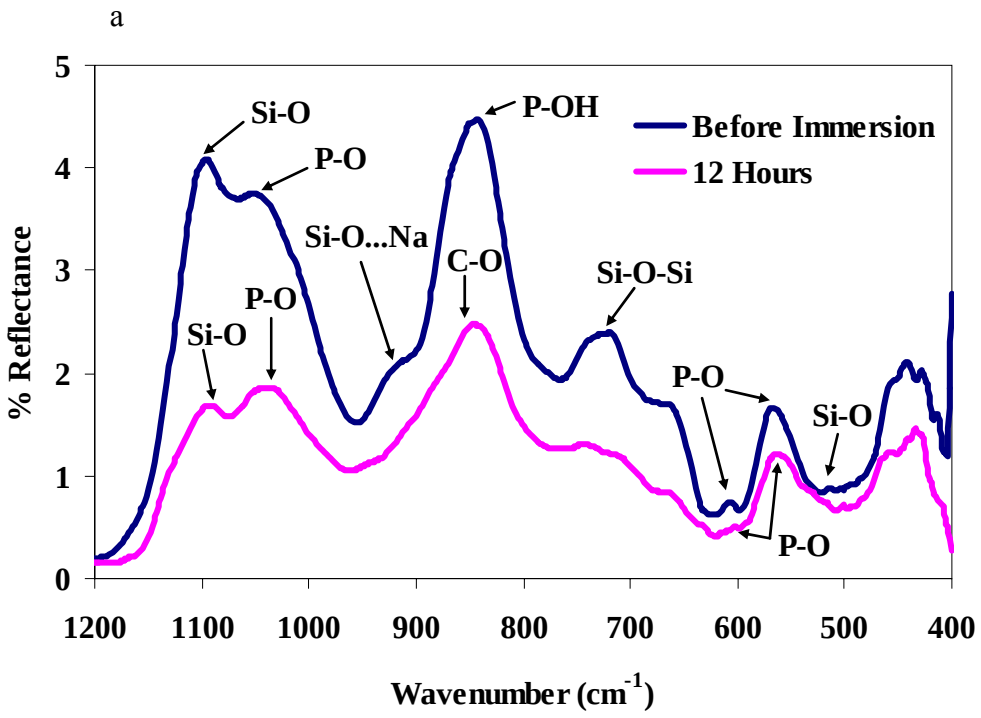

Figure 3.2.2 (a-c): FTIR Results

FTIR results show that after 12 hours of immersion in SBF, the surface of the SCPC disks was altered similarly for all three thermal treatment temperatures. Characteristics of a HA later are noted by the P─O peaks at 568 and 1052 cm^{-1}, and the shoulder at 605 cm^{-1}. In addition, the Si─O peaks decreased on the surface of the SCPC disks which correlates with the ICP results (Figure 3.2.1 (c)). (a) Disks thermally treated at 800 ºC.

b

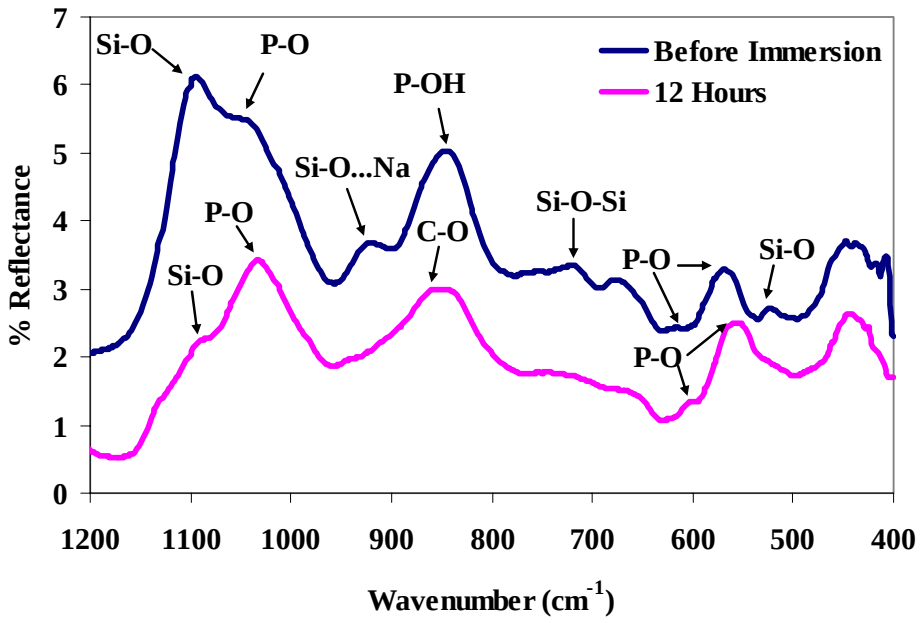

c

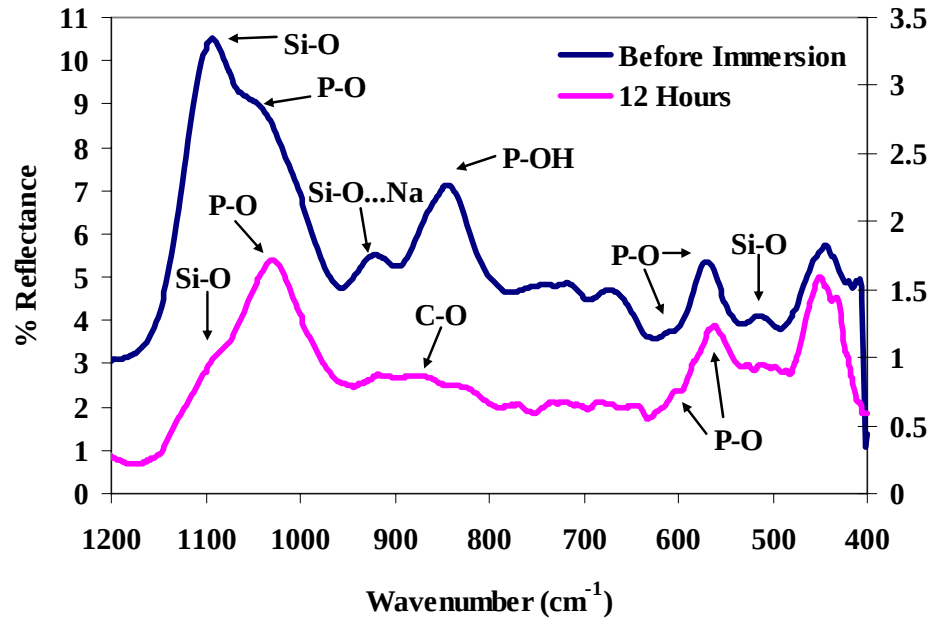

Figure 3.2.2 (a-c): FTIR Results (continued)

FTIR results show that after 12 hours of immersion in SBF, the surface of the SCPC disks was altered similarly for all three thermal treatment temperatures. (b) Disks thermally treated at 850 ºC. (c) Disks thermally treated at 900 ºC.

3.2.3 Surface Modification

The SEM micrographs in Figure 3.2.3 (a-c) confirms the formation of a HA layer on all SCPC disks after 12 hours of immersion in SBF. The SEM micrograph (Figure 3.2.3 (a)) of the SCPC disk treated at 800 ºC shows a HA layer that is in its early stages of development. The apatite crystals are dense but they are small. This correlates with the FTIR spectra that show P─O peaks that are characteristic of HA formation but that are not strong peaks. The micrograph (Figure 3.2.3 (b)) shows that the apatite formation on the surface of the SCPC disk thermally treated at 850 ºC is denser and more developed than the other thermal treatment temperatures. The surface of the SCPC disk is not visible through the apatite formation. The FTIR spectra shows the P─O shoulder at 605 cm^{-1} to be more defined for the SCPC disk thermally treated at 850 ºC, which distinguishes the apatite layer seen in Figure 3.2.3 (b). For the 900 ºC disk, the HA crystals are large (Figure 3.2.3 (c)), but the surface of the SCPC disk can be seen. Again, the FTIR spectra confirmed the formation of the HA layer on the surface of the SCPC disk thermally treated at 900 ºC.

After 1 day of immersion in SBF, the SEM micrographs (Figure 3.2.3 (d-f)) show HA layers that are more developed and that fully cover the surfaces of the thermally treated SCPC disks. The formation of the HA layer is confirmed by FTIR results (Figure 3.2.2 (a-c)) and correlates well with the significant decrease in the Ca concentration of the SBF during immersion.

3.3 SCPC-rhBMP-2 Hybrid Implantation

3.3.1 Radiographs

Data from a CT scan that was performed 4 weeks postoperatively on the rabbit ulna that was implanted with an 850 ºC thermally treated SCPC-rhBMP-2 hybrid, was converted into STL format allowing for a 3-D view of the bone. Figure 3.3.1 (a-b) shows that over 65% of the critical sized defect, initially 10 mm long, has been replaced by newly formed bone. The CT scan images show the significant bone healing and regeneration, as well as

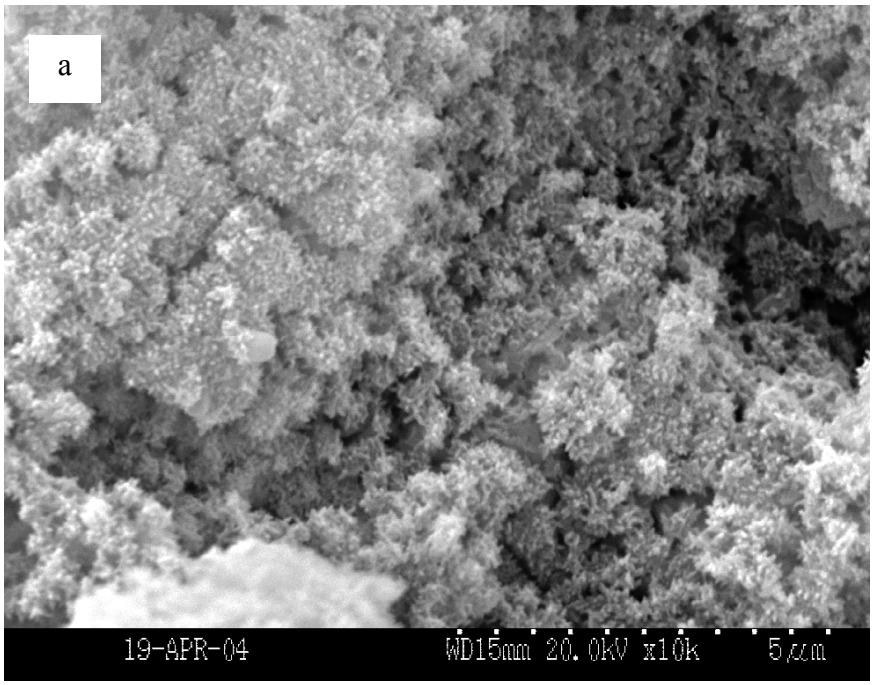

Figure 3.2.3 (a-f): SEM Micrographs After Immersion

SEM micrographs of the SCPC disk surface show that for all thermal treatment temperatures a HA layer had formed after only 12 hours of immersion in SBF. After 24 hours of immersion, these layers became denser. (a) Disks treated at 800 ºC show a dense layer of small apatite crystals (2 μm) after 12 hours of immersion.

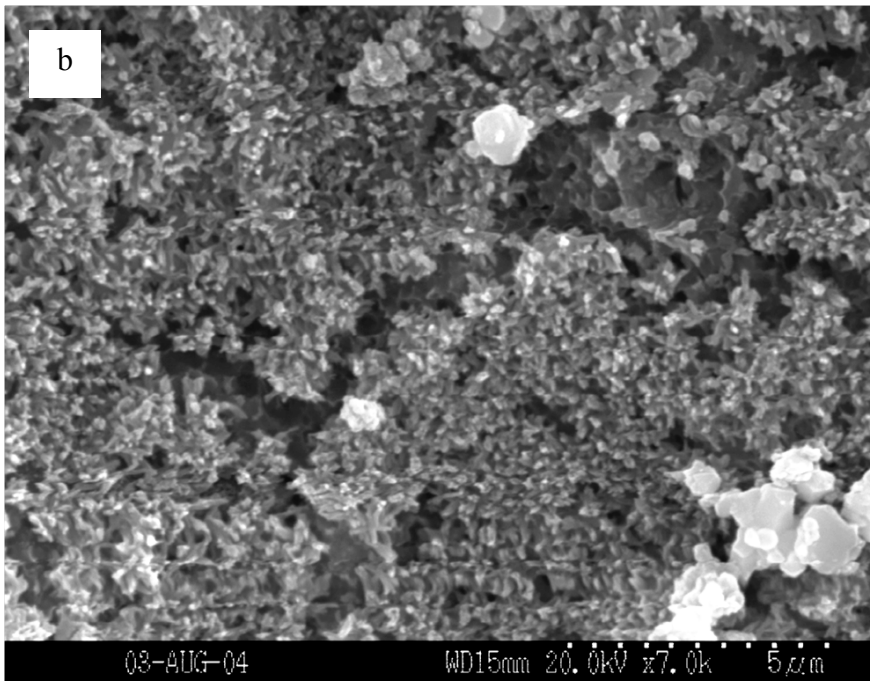

Figure 3.2.3 (a-f): SEM Micrographs After Immersion (continued)

SEM micrographs of the SCPC disk surface show that for all thermal treatment temperatures a HA layer had formed after only 12 hours of immersion in SBF. After 24 hours of immersion, these layers became denser. (b) Disks treated at 850 ºC show larger apatite crystals (5 μm) that cover the surface.

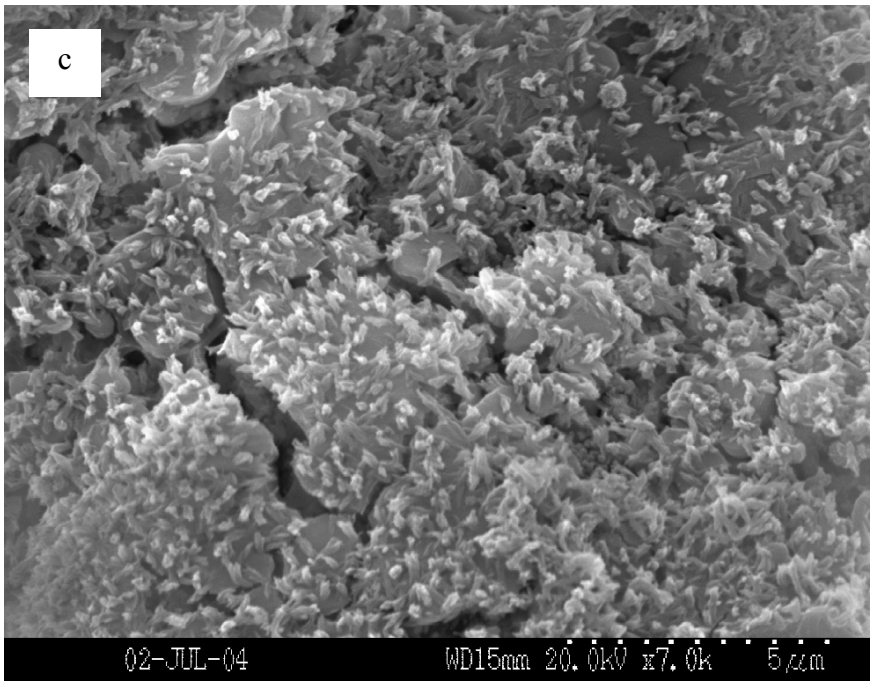

Figure 3.2.3 (a-f): SEM Micrographs After Immersion (continued)

SEM micrographs of the SCPC disk surface show that for all thermal treatment temperatures a HA layer had formed after only 12 hours of immersion in SBF. After 24 hours of immersion, these layers became denser. (c) Large apatite crystals (5 μm) are less dense on the disks treated at 900 ºC.

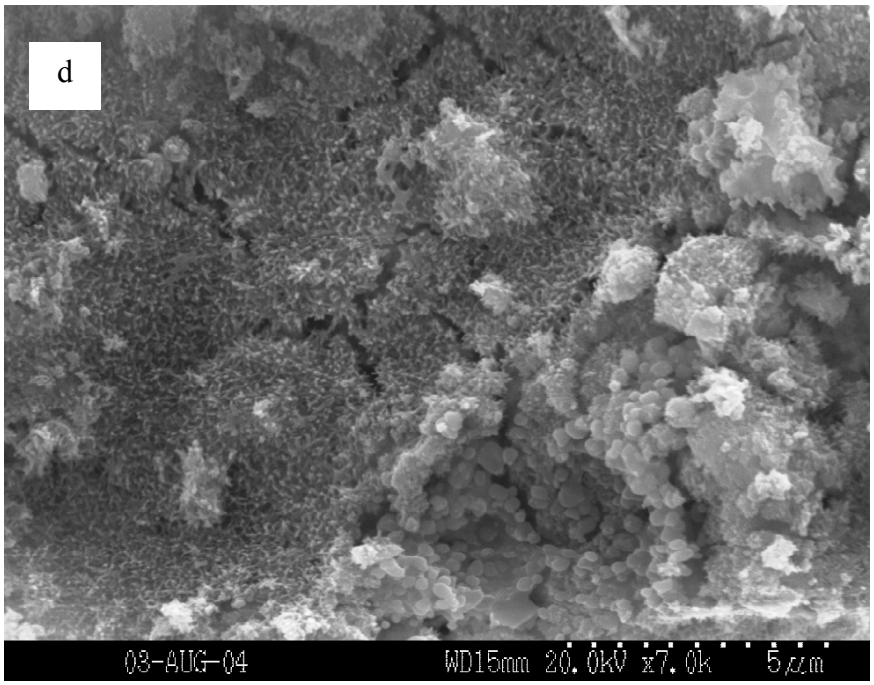

Figure 3.2.3 (a-f): SEM Micrographs After Immersion (continued)

SEM micrographs of the SCPC disk surface show that for all thermal treatment temperatures a HA layer had formed after only 12 hours of immersion in SBF. After 24 hours of immersion, these layers became denser. (d) After 24 hours of immersion, the 800 ºC disks a more dense formation of the smaller apatite crystals.

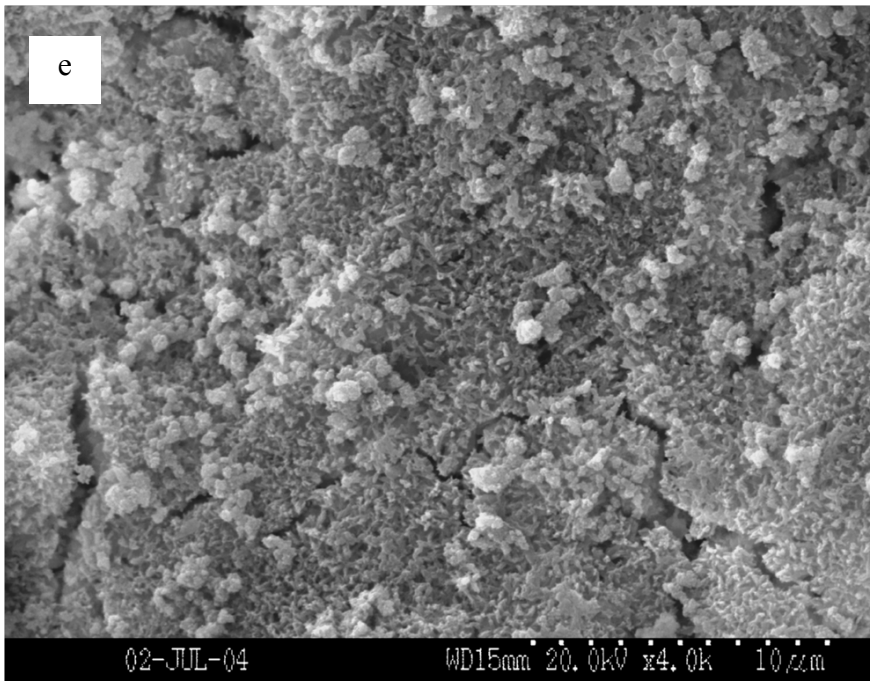

Figure 3.2.3 (a-f): SEM Micrographs After Immersion (continued)

SEM micrographs of the SCPC disk surface show that for all thermal treatment temperatures a HA layer had formed after only 12 hours of immersion in SBF. After 24 hours of immersion, these layers became denser. (e) The disks treated at 850 ºC have a thick apatite layer consisting of large apatite crystals.

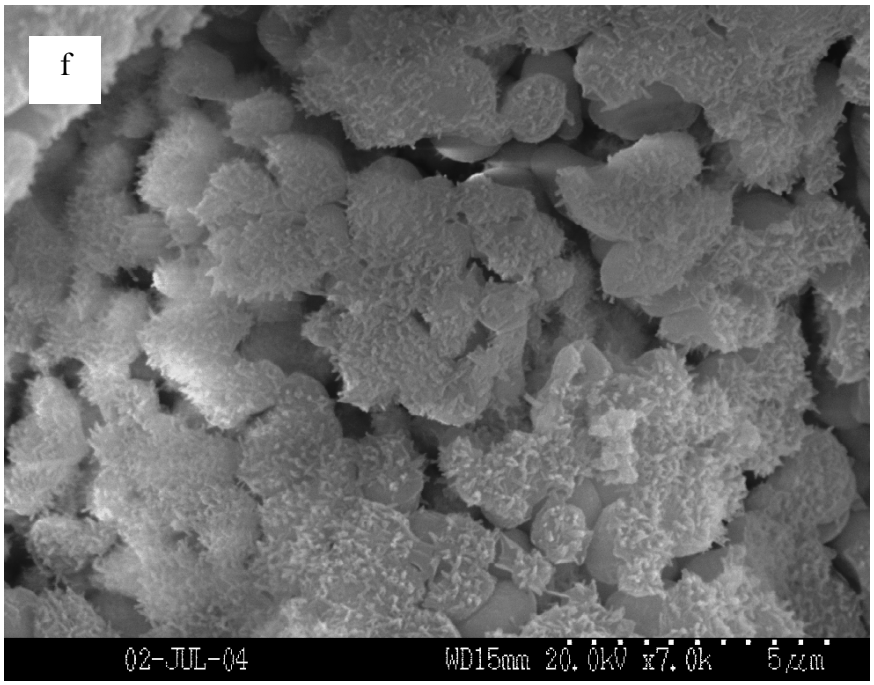

Figure 3.2.3 (a-f): SEM Micrographs After Immersion (continued)

SEM micrographs of the SCPC disk surface show that for all thermal treatment temperatures a HA layer had formed after only 12 hours of immersion in SBF. After 24 hours of immersion, these layers became denser. (f) The large apatite crystals cover more of the surface, but the SCPC material can still be seen through the hydroxyapatite layer. These results are consistent with the ICP and FTIR results (Figure 3.2.1 (a-d) and 3.2.2 (a-c)).

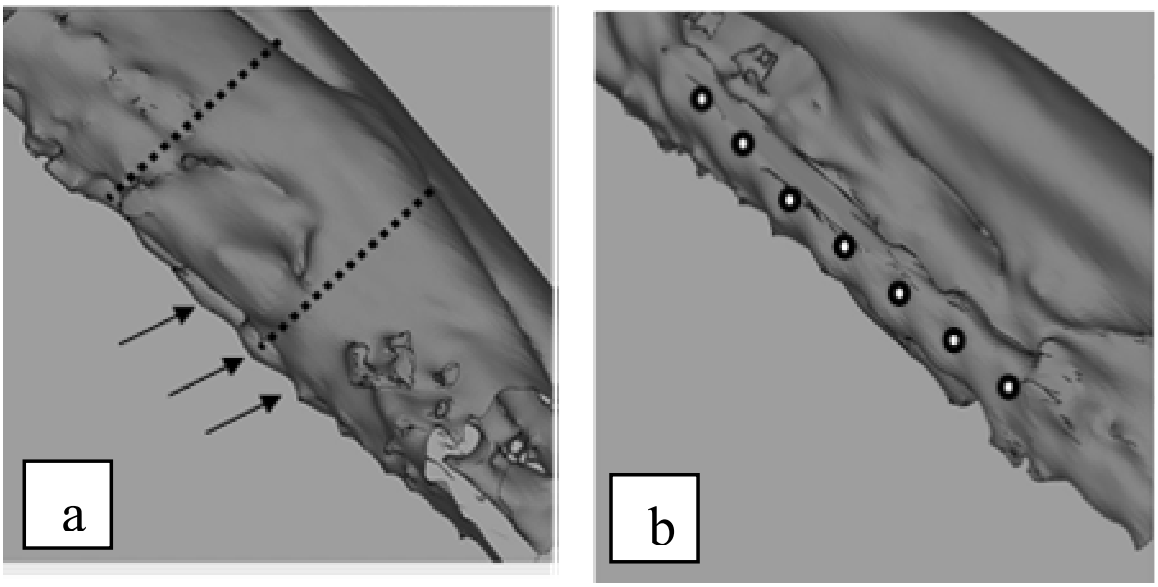

Figure 3.3.1 (a-d): Radiographic Evaluation

Initially a 10 mm long segmental defect was created in the ulna. (a) The dashed lines refer to the original edges of the defect, and the arrows point to the plate that was used to provide the initial support in the leg. Approximately 65% of the implant has been replaced by regenerated bone. (b) This shows the healing on the other side of the ulna defect. The black circles represent the place of the screws inserted into the plate to provide initial fixation and stability.

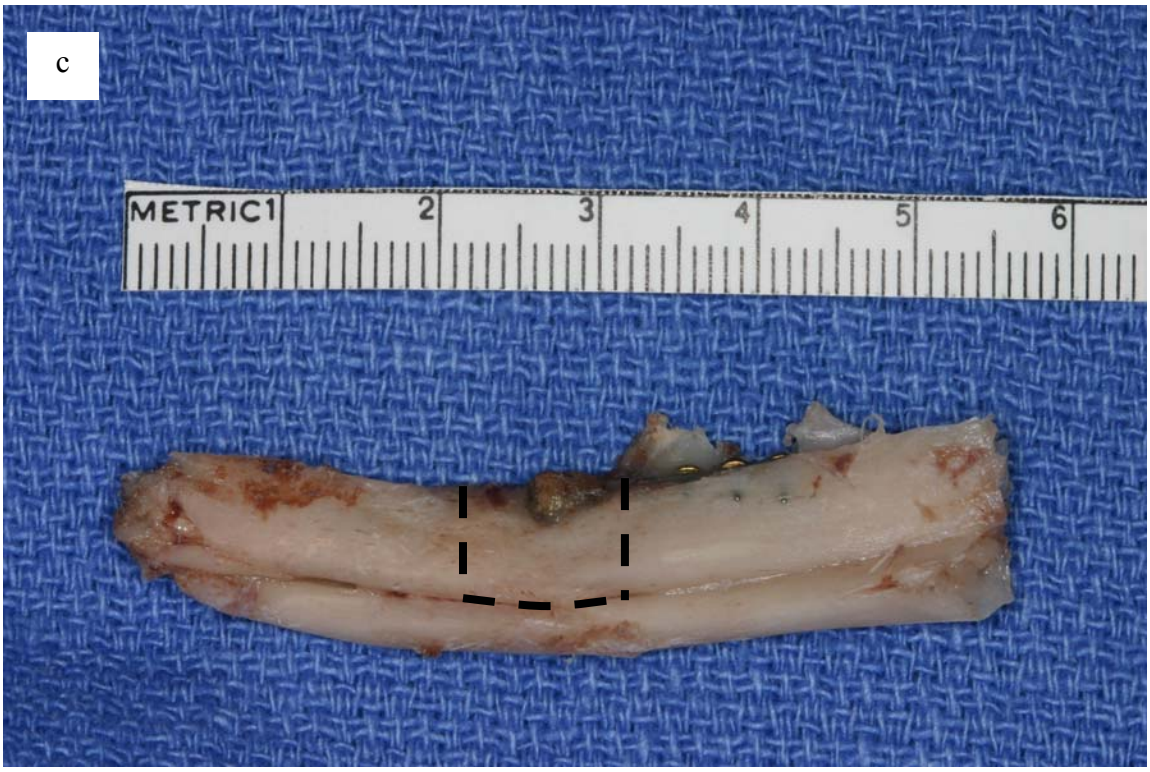

Figure 3.3.1 (a-d): Radiographic Evaluation (continued)

Digital images were taken of the rabbit ulna grafted with the SCPC-rhBMP-2 hybrid implant 16 weeks post-operative. (c) This image shows the superior side of the ulna and radius which have become fused during the healing of the 10 mm defect (dashed lines refer to the original edges defect). The implant can barely be distinguished from the bone due to the abundant formation of new bone. In this regenerated bone the high vascularization can be seen.

Figure 3.3.1 (c-d): Radiographic Evaluation (continued)

Digital images were taken of the rabbit ulna grafted with the SCPC-rhBMP-2 hybrid implant 16 weeks post-operative. (d) Exceptional healing on the inferior side of the ulna can also be seen. After 16 weeks the resorbable implant shows near complete healing of the defect. These images confirm the *in-vitro* results that showed the SCPC implant to be both bioactive and resorbable.

full implant integration, all which can be observed non-invasively during the healing process.

After 16 weeks post-operative, the rabbit was euthanized and the ulna was harvested and the surrounding tissue was removed. Digital images of the superior and inferior sides of the ulna show almost complete healing of the 10 mm critical sized segmental defect (Figure 3.3.1 (c-d)). Figure 3.3.1 (c) also shows the large amount of vascularization taking place in side the new bone formation.

3.3.2 Histology

After 16 weeks of implantation, the segmental defect in the rabbit ulna implanted with the 800 ºC thermally treated SCPC-rhBMP-2 hybrid was filled with mature bone and osteocytes. Histological analysis of the grafted ulna shows abundant bone formation, and bony bridging of the defect can be observed (Figure 3.3.2 (a-b)). Some remnants of the SCPC biomaterial are present, with bone formation directly on their surface. In general, these remnants are incorporated in newly formed bone, and no inflammatory reactions could be detected. The mature bone is also highly vascularized evident by the numerous blood vessels filled with red blood cells. In addition, osteoblasts can be seen actively forming new bone.

3.3.3 Torsional Testing

Table 3.3.3 is a summary of the torsional testing results comparing the ulna implanted with a 900 ºC thermally treated SCPC-rhBMP-2 graft to the ungrafted rabbit ulna. The mechanical testing of the ulna grafted with the SCPC-rhBMP-2 hybrid (n=3) as compared to the control ulna with no graft (n=3) shows that the maximum torsional load to failure is significantly higher ($p<0.04$) for the ulna grafted with the SCPC-rhBMP-2 hybrid. In comparing the angle at failure there is not a significant difference between the grafted and ungrafted ulna. These results are normalized for the cross-sectional area which is greater for the grafted ulna which has fused with the radius.

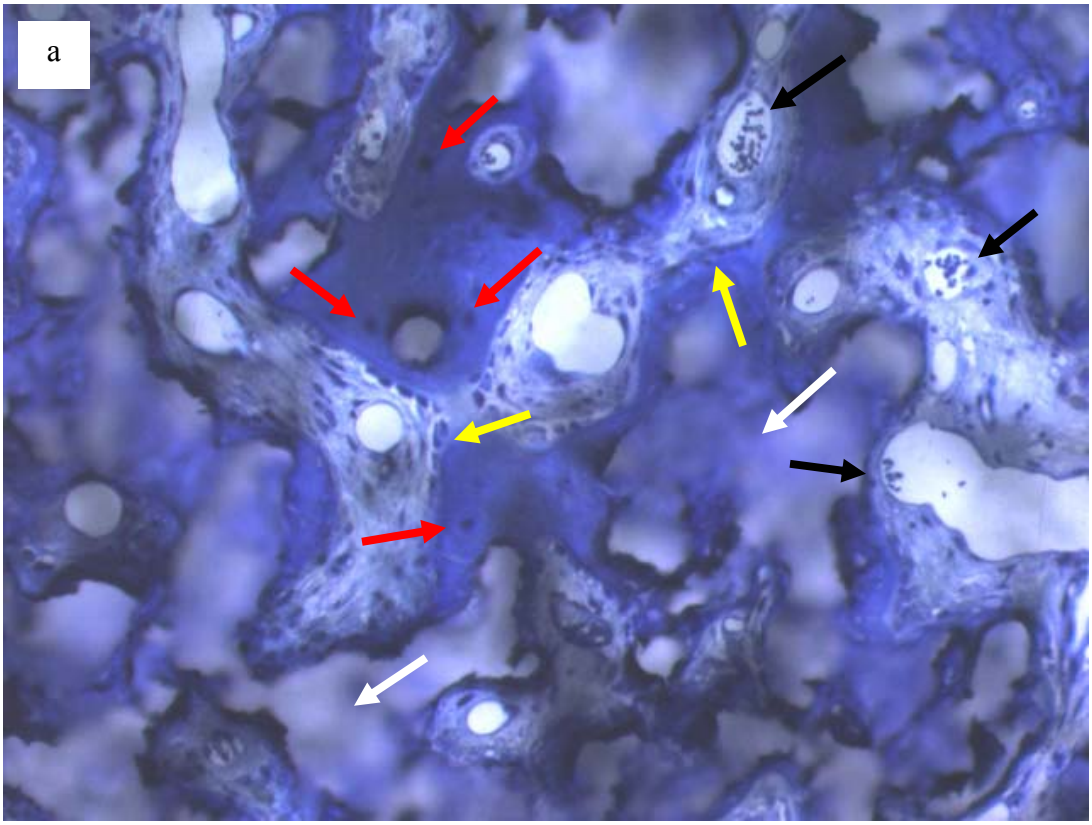

Figure 3.3.2 (a-b): Histological Analysis

Histological analysis of the rabbit ulna after 16 weeks of implantation showed that the SCPC-rhBMP-2 implant had been replaced by regenerated mature bone. (a) This image shows that the regenerated bone is highly vascularized. Black arrows point to the blood vessels containing red blood cells indicating vascularization of the regenerated bone tissue. In addition, osteocytes (red arrows) can be seen in the mature mineralized tissue. Remnants of the SCPC material (white arrows) are incorporated in the newly formed bone and osteoblasts (yellow arrows) can be seen actively forming new bone.

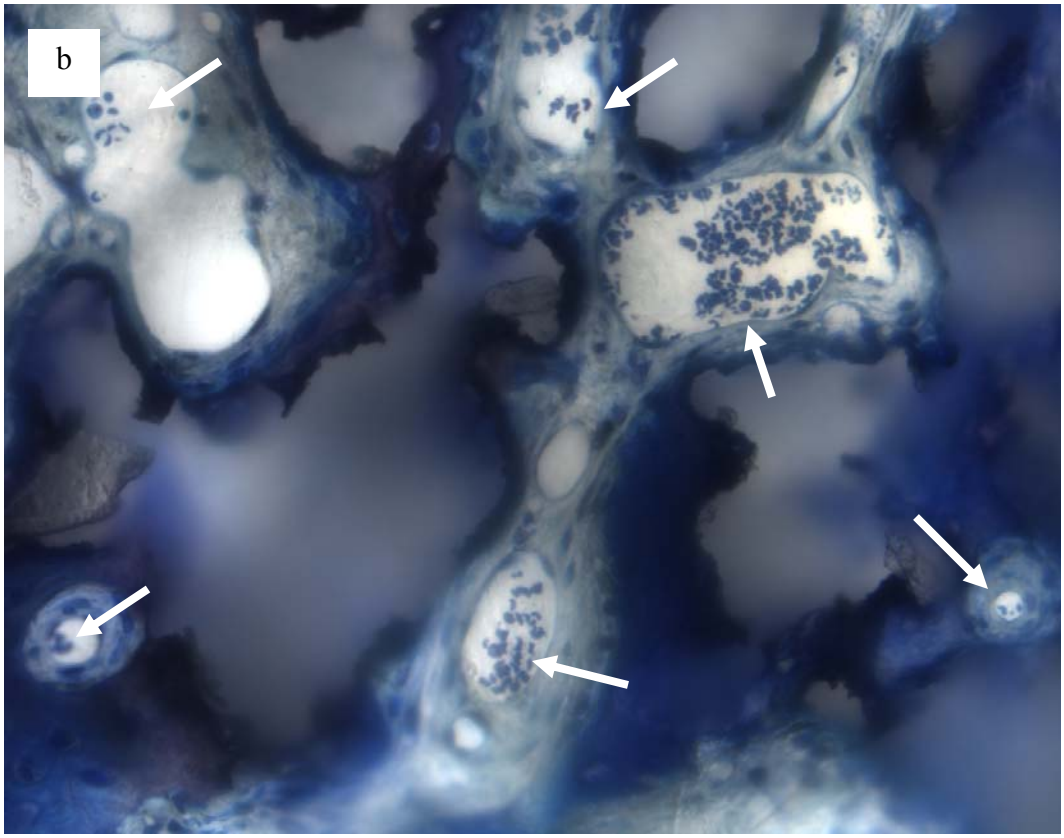

Figure 3.3.2 (a-b): Histological Analysis (continued)

Histological analysis of the rabbit ulna after 12 weeks of implantation showed that the SCPC-rhBMP-2 implant had been replaced by regenerated mature bone. (b) A closer look shows the large number of red blood cells (white arrows) in the regenerated bone.

Table 3.3.3: Torsional Testing Results

Torsional testing of the ulna grafted with the SCPC-rhBMP-2 hybrid and the ungrafted ulna showed that the maximum torsional load to failure was significantly greater ($p<0.04$) for that of the grafted ulna. However, there was not a significant difference between the angles at failure for the grafted ulna as compared to the ungrafted ulna.

	Maximum Torque (Nm)		Angle at failure (rad)	
	Ungrafted	Grafted	Ungrafted	Grafted
Rabbit No.				
1	13.4	16.457	0.43	0.195
2	5.359	25.099	0.285	0.608
3	3.92	18.652	0.249	0.541
Mean ± SD	7.56 ± 5.11	20.07 ± 4.49	0.32 ± 0.10	0.45 ± 0.22
p	0.04*		0.43	
*indicates significant difference				

Chapter 4

Discussion

4.1 *In-Vitro*

Through *in-vitro* testing, the porous, resorbable, bioactive SCPC material was found to possess both the physical and biological characteristics required to make it a suitable carrier system for the delivery of rhBMP-2 in a segmental bone defect. The SCPC material demonstrated high porosity and large pores that were interconnected. Compression testing showed that although the material was porous, the mechanical strength was similar to that of trabecular bone. Upon immersion in a physiological solution, the composite slowly degraded while at the same time a HA layer precipitated onto its surface. After loading the SCPC with rhBMP-2, the hybrid demonstrated a sustained release profile for 14 days in a physiological solution.

4.1.1 Material Characterization

SEM micrographs of the bioactive SCPC samples, processed by the Z-Corp 3-D printer and then thermally treated, showed the samples to be highly porous, providing a large surface area for enhanced tissue ingrowth (Figure 3.1.1 (a-d)). The interconnectivity of the pores creates a scaffold that allows for cell and nutrient migration throughout the entire SCPC sample. If the pores are not interconnected, the cells can only survive at the surface of the sample, thus vascular and bone ingrowth will never occur.

Since the viability of the regenerated bone depends upon the rate of vascularization it is critical that the scaffold be porous. In fabricating a biomaterial to replace bone, the intent is for the internal structure of the scaffold to mimic that of bone. The porosity of cortical bone ranges from 5% to 30% while cancellous bone porosity ranges from 30% to 90% [40]. The high porosity of SCPC, 44-54%, facilitated the ingrowth of fibrovascular tissue

that then ossified and the large pore size range (4 nm-356 μm) of the SCPC scaffold allowed for cell invasion, vascularization, and nutrients to reach the invaded cells so that bony ingrowth and osseous integration could occur (Figure 3.3.2 (a-b)). Although initially it was weaker from a structural standpoint, the porous SCPC material has an advantage over a solid material in that the pores facilitate the ingrowth of fibrovascular tissue that then ossified. On the other hand, a nonporous implant would not allow for the invasion of blood vessels and cells due to its compact structure.

A previous study showed that mineralized bone growth into porous implants requires a minimum interconnective pore size of 100 μm, the ingrowth of osteoid tissue requires a minimum pore size between 40 and 100 μm, and the ingrowth of fibrous tissue requires a minimum pore size between 5 and 14 μm [41]. However, another study reported that not only a pore size of greater than 50 μm is necessary, but the interconnections play an important role in bone formation as well [42]. That study reported that to allow for cell penetration the interconnections size must be greater than 20 μm. Yet, if a material is resorbable, its pore and interconnection sizes will be modified by degradation upon contact with a physiological solution. For the SCPC scaffold, although the initial pore size range was 4 nm-356 μm, and the interconnections range was from 10 μm-50 μm, the immediate resorption that took place in a physiological solution increased this pore size range and interconnection size, and synergistically increased the pathways for cell invasion and vascularization to take place.

Different thermal treatment temperatures of the SCPC composite showed that for different temperatures, the overall pore and interconnection sizes remained very similar. However, the distribution of these pore sizes was affected by the thermal treatment. The pore size ranges that were shown to be affected by the thermal treatment were 10 μm-25 μm and 25 μm-100 μm (Table 3.1.2). In addition, as the sintering temperature was increased, the porosity percent was decreased. This was due to a greater amount of fusion between the particle edges, and although the pore sizes were not changed, the porosity percent was decreased with increasing temperature. The decrease in the porosity percent of the SCPC is directly related to the surface area, which also decreased with

increasing thermal treatment temperature. Nevertheless, due to SCPC being a resorbable biomaterial, the differences in porosity and pore size distribution due to different thermal treatment temperatures are negligible. Upon immersion in a physiological solution, the material begins to be resorbed and the pore sizes and porosity immediately changed.

4.1.1.1 Hydroxyapatite Layer

Moreover, the high porosity of SCPC provided a high surface area in contact with tissue fluids and cells, which in turn enhanced the dissolution/precipitation reactions at the material surface, leading to the formation of a HA layer (Figure 3.2.3 (a-c)). The dissolution of the SCPC *in-vivo* occurred in two ways, solution-mediated resorption and cell-mediated resorption. The solution-mediated resorption involved the dissolution/precipitation reaction that occurred as the exchange of ions took place between the SCPC and the physiological solution. The cell-mediated resorption involved the stimulation of osteoclastic resorption of SCPC as seen in Figure 3.3.2 (a). To meet the requirements of skeletal growth and mechanical function, bone constantly undergoes dynamic remodeling by a coupled process of bone resorption by osteoclasts and reformation by osteoblasts. This cell-mediated resorption also occurred upon implantation of the SCPC implant in rabbit ulna defect; osteoclasts broke down the SCPC while the osteoblasts formed new bone in its place (Figure 3.3.2 (a)).

Immersion of SCPC in a physiological solution led to formation of an HA layer, which precipitated onto its surface, as shown by FTIR (Figure 3.2.2 (a-c). The formation of this HA layer is essential to new bone formation because hydroxyapatite's chemical and crystallographic structure is very similar to that of bone mineral. When immersing a biomaterial, such as SCPC, in a physiological solution the surface chemical reactions result in the formation of this HA layer to which bone can bond more readily. Therefore, the essential requirement for a biomaterial to bond to living bone is the formation of a bone-like apatite layer on its surface *in-vivo*. One previous study has proven that the SBF, having almost the same ionic concentration as human blood plasma, can reproduce the surface changes *in-vivo* [39]. In addition, the precipitation of a HA layer after immersion

in SBF has been widely used to assess the degree of bioactivity of a biomaterial [22]. Thus, investigating the biological behavior of bioceramics in SBF is considered to be the most efficient method to authenticate their bioactivity in the body environment.

4.1.1.2 Mechanical Strength

In replacing bone in a segmental defect, it is important for a porous implant to have initial mechanical strengths that will allow it to withstand loading until bone regeneration can occur. A biomaterial must demonstrate equivalent mechanical properties to the type of bone being replaced, whether it is trabecular or compact bone. However, by virtue of the need of porosity and resorbability there would be a trade off between the mechanical strengths and the porosity. This is due to the compressive strength being inversely proportional to the volume percentage of porosity. Mechanical testing of the thermally treated SCPC material confirmed that although the samples were porous, their compressive strengths (5-15 MPa) were similar to that of trabecular bone (2-12 MPa) (Table 3.1.3). The high compressive strength of SCPC was due to the high thermal treatment temperature of the SCPC samples which caused the particle edges to fuse with each other during the sintering reaction. As the thermal treatment was increased the mechanical strengths of the material also increased, due to greater fusion of the SCPC particle edges. However, this increase in strength corresponded to a decrease in porosity as previously mentioned. Nevertheless, the compressive strengths of the SCPC samples were similar to trabecular bone, but less than that of compact bone which has a compressive strength of (100-220 MPa). Therefore if it used for cortical bone replacement, as in this study, an external fixation device should be used to provide the initial support. Then as the porous SCPC implant undergoes biodegradation, it is slowly replaced by bone. The strength of the implant in the defect will gradually increase as the new bone grows into the porous network of the SCPC implant. Although a nonporous or compact scaffold would have higher mechanical properties, as previously stated, a solid material would not allow for the invasion of cells and blood vessels that are necessary for new bone to form. In addition, it used as a carrier for growth factors, a solid scaffold

would cause immediate release of the growth factor, instead of a desired controlled release.

4.1.1.3 Geometry

For a bone tissue engineering scaffold to successfully regenerate bone in a defect and be capable of supporting cell proliferation, its internal as well as external geometry must replicate natural bone [40]. By fabricating the SCPC using the Z-Corp processing, a SFF technology, a scaffold that mimics the internal and external architecture of natural bone was created. Upon implantation *in-vivo* this scaffold acted as a placeholder for the induction of new bone. As can be seen in Figure 3.3.1 (c-d), bone mass developed in the size and shape of the Z-Corp processed SCPC scaffold. The external shape and topography of natural bone is very complex; no bone in the body is perfectly square or cylindrical. This is why it is necessary to fabricate bone tissue engineering scaffolds that exactly replicate bone. Z-Corp processing of the SCPC material allowed for this.

4.1.2 rhBMP-2 Release Kinetics

When a bone tissue engineering scaffold is used as a carrier for BMP, it must have a controlled release of the BMP, so that the protein is retained at the grafted site for a period of time sufficient to stimulate cell differentiation and induce bone formation. It is desirable to have a bulk release of BMP initially, followed by a more gradual release thereafter [20]. Many studies have investigated the ability of calcium phosphate ceramics to serve as a delivery system for BMP [9, 43, 44]. However, these studies showed that the porous ceramic implants demonstrated a very limited release of rhBMP-2. This means that almost all of the rhBMP-2 was maintained at the cement surface, inhibiting the protein from exerting its biological action. In our study, upon immersion in a physiological solution, the SCPC-rhBMP-2 hybrid implant demonstrated a continuous release of rhBMP-2 for 14 days (Figure 3.1.4). As compared to HA, the SCPC implant had a greater release of rhBMP-2 over the 14 day period. Due to the high porosity and

the nanopores of the SCPC implant, the protein had a large surface area with which to adsorb. The nanopores (Figure 3.1.1 (d)) allowed for a greater surface area for protein adsorption, they provided protective pockets for the adsorbed protein, and enhanced the sustained release of rhBMP-2 [45]. This sustained release of rhBMP-2 by SCPC was demonstrated *in-vivo*, where the SCPC implant maintained the growth factor at the defect, stimulating osteoblast differentiation and new bone formation (Figure 3.3.2 (a)).

4.1.3 Interaction of SCPC with SBF

4.1.3.1 Effect of Immersion Duration

ICP analyses indicated that after immersing the resorbable SCPC samples in SBF the Ca concentration of the SBF decreased linearly until 12 hours while the P, Si and Na concentrations of the SBF increased (Figure 3.2.1 (a-d)). Figure 3.2.1 (a) shows the initial decrease in the Ca concentration which was due to the precipitation of a HA layer onto the surface of the SCPC as has been confirmed by FTIR (Figure 3.2.2 (a-c)) and SEM (Figure 3.2.3 (a-f)). FTIR analyses showed that after 12 hours SCPC had developed a layer consisting of small HA crystallites that completely covered its surface. SEM analyses showed the homogenous distribution of these HA crystals, having a size of 1 μm, on the surface and in the pores and interconnections. Another study found similar results when the biomaterial hydroxyapatite was immersed in SBF [46]. They found that after 1 day the hydroxyapatite surface was completely covered by a layer of precipitates that nucleated on the surface and in the pores and chasm.

For SCPC, the precipitation of the HA layer occurred concurrently with the initial dissolution of the ions from the samples. The previously mentioned study with the hydroxyapatite biomaterial also found that the dissolution of Ca and P and the precipitation of calcium phosphate occur concurrently, leading to the HA layer on its surface. Another study investigated the dissolution behavior of HA/BG in SBF [47]. This study found that at the early stage of immersion, the dissolution preceded faster than the

eventual precipitation of an apatite layer. In the case of SCPC, as the immersion time increased beyond 12 hours the Ca concentration of the SBF began to plateau. This was due to an equilibrium being reached between the precipitation/dissolution interaction of the SCPC sample and the SBF. This equilibrium exchange of ions indicates the constant degradation of the resorbable SCPC implant being replaced by a bone-like apatite layer that formed after just 12 hours of immersion in SBF. In contrast, the study with the hydroxyapatite biomaterial did not show an equilibrium exchange of ions until after 14 days of immersion.

In contrary to the initial decrease in the Ca concentration of the SBF, the P concentration initially increased (Figure 3.2.1 (b)). The increase in P concentration of the SBF may be due to the fact that not all P ions dissolved from the SCPC sample were consumed in the formation of the HA surface layer. SCPC initially has a Ca to P ratio of 1, however when Ca and P precipitated after dissolution they precipitated as hydroxyapatite which has a Ca to P ratio of 1.67. Therefore, the exchange of the Ca and P ions between the SCPC sample and the SBF resulted in excess P ions in the SBF that were not involved in the mechanism of the formation of apatite on the SCPC surface. The P concentration began to level off after 12 hours of immersion. For the remaining immersion time, the P concentration slightly decreased and, like the Ca concentration, began to plateau. This again indicates that equilibrium in the precipitation/dissolution interaction had been reached. The study involving the hydroxyapatite biomaterial showed an initial increase in P concentration of SBF, and then a decrease. Like the Ca ions, an equilibrium exchange of P ions for the hydroxyapatite biomaterial was not reached until 14 days of immersion.

As the immersion time increased the amount of CaP precipitated onto the SCPC sample also increased, creating a dense HA layer on the surface. Moreover, the FTIR spectra after 12 hours also showed signals characteristic of a carbonate hydroxyapatite layer that was noted by the peaks for P─O at 560, 605, and 1030 cm^{-1} (Figure 3.2.2 (a-c)). Other studies have attributed these same peaks as the P─O bonds of HA [45, 48-51]. This, in conjunction with the ICP results, demonstrates that the dissolution of the SCPC in

physiological solution was followed by the formation of a hydroxyapatite layer known to stimulate bone cell function. Similar studies of the effect on the interaction of hydroxyapatite and bioactive acrylic-glass samples with SBF showed that after 24 hours and 4 days, respectively, there was a HA layer formed on the surface [46, 52]. The formation of the HA layer on the SCPC samples after only 12 hours shows the higher bioactivity of the material. In conjunction, SEM micrographs confirm that after 12 hours of immersion in SBF, there is formation of a HA layer on the SCPC samples. Micrographs after 1 day of immersion show a denser HA layer formed that fully covered the surface of the SCPC samples.

It is also important to note that when the dissolution of the ions from the SCPC sample takes place, they do not only dissolve from the outer surface of the SCPC but also throughout the sample. Due to the sample being porous, the SCPC sample can degrade evenly throughout and the ions from the SBF precipitate throughout the entire SCPC sample, inside and out. This means that the formation of an HA layer not only occurs on the outside surface of the SCPC sample, but also throughout the network of pores that make up the SCPC sample.

The ICP analyses indicated that the Si concentration of the SBF was initially very low but showed a linear increase for the duration of the SCPC sample being immersed in the SBF (Figure 3.2.1 (c)). This increase in Si concentration of the SBF reflects the dissolution of Si ions from the SCPC sample into the SBF. Analysis of the SCPC surface chemistry by FTIR showed that before immersion in the SBF, the SCPC samples had strong Si─O peaks due to the silica-rich composition. After 12 hours of immersion in the SBF, these peaks were no longer distinct. This correlates with the ICP results which showed an increase in the Si concentration of the SBF after 12 hours. This proves that the Si was released from the SCPC sample into the immersion solution. Previous studies reported that the high bioactivity of silicon [53] which when released nucleated HA formation apart from the SCPC samples. In addition, this dissolution was also beneficial in that as the silica-rich samples released the silicon, it allowed for the HA layer to form on the surface in its place. In the current study it was found that the dissolution from the SCPC

allowed the Si ions to nucleate apatite formation away from the SCPC sample as well as allowing the Ca and P ions to create an HA layer on and throughout the SCPC in its place. Previous studies that have used polymers as a tissue engineering scaffold, "impregnate" their material with sodium silicate gel, which acts as a nucleating agent to promote the nucleation and growth of a HA layer on the polymer surface [54, 55]. On the other hand, one study reported that apatite cannot precipitate on silica-rich surfaces [56]. Consequently, the dissolution of the Si from the SCPC samples not only nucleated apatite formation away from the implant, but it in its absence allowed for apatite formation on the surface of the implant.

SEM analysis after immersion in SBF confirms the morphology changes of the SCPC surface that were demonstrated in the ICP and FTIR results. Micrographs show that these surface modifications were in the form of HA crystal deposits that cover the surface of the SCPC scaffold and on the surface.

4.1.3.2 Effect of Thermal Treatment Temperature

The thermal treatment temperature of the SCPC samples had a significant effect on the interaction between the SCPC and SBF. The significant differences in the corrosion behavior of the SCPC disks are due to the different thermal treatment they were subjected to. Each of the thermal treatments causes the SCPC disks to have diverse crystalline phases. Each of the phases responds differently to being immersed in the SBF and these differences are shown in the varied ionic concentrations of the SBF at each of the immersion time periods. ICP results show that with respect to P, and Si, ion precipitation/dissolution, the SCPC samples thermally treated at 850 ºC demonstrated a significantly higher corrosion rate than those samples treated at 800 or 900 ºC (Figure 3.2.2 (a-c)). In conjunction, FTIR spectra showed that after immersion in SBF, the appearance of peaks for P─O, observed at 560, 605, and 1030 cm^{-1}, which are characteristics of carbonate hydroxyapatite, were more prominent for those samples thermally treated at 850 ºC as compared to the other thermal treatment temperatures. Furthermore, SEM micrographs confirm the formation of a HA layer, showing that SCPC

samples thermally treated at 850 ºC have a denser apatite layer formed with larger apatite crystals (Figure 3.2.3 (a-f)). The significant differences in the corrosion behavior of the SCPC samples were due to the different thermal treatment temperatures they were subjected to. Each of the thermal treatments caused the SCPC samples to have diverse crystalline phases. Each of the phases responded differently to being immersed in the SBF and these differences are shown in the varied ionic concentrations of the SBF at each of the immersion time periods.

The results of the Material Characterization together with the Interaction of SCPC with SBF show that the SCPC processed with the Z-Corp 3-D printer is highly porous with a large surface area and high compression strength and is not only bioactive but is also resorbable. All of these attributes combined form a scaffold that can serve as a tissue engineering substitute for autologous bone implant.

4.2 *In-Vivo*

After obtaining successful results through the *in-vitro* testing of SCPC, the porous, resorbable, bioactive biomaterial was tested *in-vivo* as a carrier for rhBMP-2. The SCPC-rhBMP-2 hybrid prepared by a rapid prototyping technique enhanced rapid bone regeneration in a segmental bone defect in the ulna of rabbit. Implantation of the SCPC-rhBMP-2 hybrid into a segmental defect created in the ulna of rabbit showed that after 3 months the resorbable implant had been replaced with new bone and the defect was almost completely reconstructed. Torsional testing demonstrated that the bone strength was returned to normal. Histological evaluation showed that the SCPC-rhBMP-2 hybrid had been replaced by mature bone that has directly formed on the implant surface. These results indicate that the SCPC-rhBMP-2 can serve as a tissue engineering alternative to autologous bone grafting.

4.2.1 Radiographs

CT scans of the rabbit ulna allowed for a non-invasive way to track the progress of the healing of the segmental defect. After 4 weeks of implantation, significant bone healing and full implant integration with bone can be observed in the defect grafted with the 850 ºC thermally treated SCPC-rhBMP-2 hybrid (Figure 3.3.1 (a-b)). In addition, direct apposition of bone onto the implant surface can be seen. After just 4 weeks of implantation, the resorbable SCPC-rhBMP-2 hybrid had induced the formation of newly formed bone that replaced about 65% of the initially 10 mm long critical sized defect. This rapid healing demonstrates the high bioactivity of the SCPC and the osteoinductive ability of the rhBMP-2 to differentiate mesenchymal stem cells into osteogenic cells. In addition, due to the SCPC-rhBMP-2 scaffold being processed using the Z-Corp 3D printer and made into an exact replica of the defect, this allowed for an intimate contact between the bone and the implant. Not only did this allow for rapid integration of cells, but the regenerated bone mass also was formed in the exact size and shape of the natural bone.

Digital images of the rabbit ulna grafted with the SCPC-rhBMP-2 hybrid harvested after 16 weeks of implantation showed almost complete healing of the defect (Figure 3.3.1 (c-d)). Due to the abundant new bone formation, it was barely distinguishable where the implant had originally been. Figure 3.3.1 (c) showed the high vascularization of the regenerated bone, indicating the integration of blood vessels throughout the entire original defect.

4.2.2 Histology

Histological analysis showed newly regenerated bone with a fully developed Haversian system. As shown in Figure 3.3.2 (a-b) the regenerated bone was highly vascularized and osteocytes could be seen in the mature mineralized tissue just 12 weeks after implantation of the SCPC-rhBMP-2 hybrid. Remnants of the SCPC biomaterial were incorporated in

the newly formed bone, with direct bone apposition on its surface. Differentiated osteoblasts were observed actively regenerating bone. A study using a combination graft of rhBMP-2/PLGA in a segmental defect, histologically showed only the abundance of immature bone after 16 weeks of implantation [57]. Another study using PLGA-coated gelatin sponge as a carrier for rhBMP-2 in a segmental defect showed similar formation of bony bridging by newly formed bone after 16 weeks [16]. However, a study that used porous polyurethane, upon histological evaluation, showed macrophages and giant cells getting organized around the edges of the porous polymer [8]. The histological evaluation of the SCPC-rhBMP-2 hybrid showed no signs of an adverse inflammatory reaction. The histological results indicate that the newly formed bone inside the defects grafted with SCPC-rhBMP-2 scaffold has all the morphological characteristics of mature bone.

4.2.3 Torsional Testing

To regain complete functionality of bone the new regenerated bone needs to have the same mechanical strengths as natural bone. As new bone is formed in place of a defect, the goal is to return the strength of the bone back to normal. Torsional strength of the rabbit ulna grafted with the 900 ºC thermally treated SCPC-rhBMP-2 hybrid was tested in comparison to the ungrafted ulna. Restoration of maximum torque and angle at failure of the regenerated bone to comparable levels of natural bone was seen after 12 weeks of implantation (Table 3.3.3). Due to the high porosity and bioactivity of SCPC and the osteoinductive capabilities of rhBMP-2, bone induction occurred rapidly and the regenerated bone became mechanically equivalent to the original bone. Although direct comparison between studies is difficult due to differences in experimental techniques, the results in this study show a similar time frame in the restoration of bone strength. Kokubo et al. used poly[L-lactide-co-glycolide]copolymer-coated gelatin sponge as a carrier for BMP in a segmental defect and achieved restoration of maximum torque and angle at failure to the intact levels after 32 weeks of implantation [13]. However, it was found in this study that the implant that had initially been processed into a block caused an increase in diameter of the regenerated bone. This was not found in our study because the SCPC-rhBMP-2 was fabricated using a Z-Corp 3D printer which allowed for an exact

replica of the defect to be made. Another study, using resorbable calcium-phosphate particles in a segmental defect, found that after 12 weeks, the bone formed in the defect had relatively poor mechanical strengths due to the resorption of the particles taking place before complete remodeling of the bone could occur [6]. The high porosity, bioactivity, and osteoinductive behavior of the SCPC-rhBMP-2 hybrid induced the rapid formation of bone, which allowed for the regenerated bone to regain complete functionality after just 12 weeks of implantation.

Chapter 5

Conclusion

Bioactive resorbable SCPC, processed using a 3D rapid prototyping technique, created highly porous scaffolds with interconnected pathways to allow for cell and blood vessel invasion. *In-vitro* testing of the SCPC material indicated that the material had high mechanical properties. In addition, when immersed in physiological solution, the SCPC material demonstrated controlled dissolution/precipitation reactions that led to the formation of a biological hydroxyapatite surface layer known to stimulate bone cell function. When loaded with rhBMP-2, the SCPC-rhBMP-2 hybrid showed a sustained release of the growth factor. *In-vivo* testing of the SCPC-rhBMP-2, prepared by a rapid prototyping technique to create an exact replica of a segment of the rabbit ulna, showed excellent bone regeneration. This hybrid enhanced bone regeneration in a segmental, load-bearing bone defect in the ulna of rabbit. Torsional testing of the ulna demonstrated the restoration of complete functionality after just 12 weeks of implantation. Histological evaluation showed differentiated osteoblasts and osteocytes in the mature mineralized tissue. The enhancement of complete bone regeneration after 16 weeks was attributed to the high bioactivity and resorbability of the material. Both the *in-vitro* and *in-vivo* results indicate that the porous, resorbable, bioactive SCPC-rhBMP-2 hybrid can serve as a tissue engineering substitute for autologous bone implant.

REFERENCES

1. Isobe M, Yamazak Y, Mori M, Amagasa T. Bone regeneration produced in rat femur defects by polymer capsules containing recombinant human bone morphogenetic protein-2. *Journal of Oral & Maxillofacial Surgery* 57, 695-698 (1999)
2. Betz RR. Limitations of autograft and allograft: new synthetic solutions. *Orthopedics* 25, S561-S570 (2002)
3. Parikh SN. Bone graft substitutes: past, present, future. *Journal of Postgraduate Medicine* 48, 142-148 (2002)
4. Suchanek W, Yoshimura M. Processing and properties of hydroxyapatite-based biomaterials for use as hard tissue replacement implants. *Journal of Materials Research* 13(1), 94-117 (1998)
5. Rawlings CE. Modern bone substitutes with emphasis on calcium phosphate ceramics and osteoinductors. *Neurosurgery* 33(5), 935-938 (1993)
6. Bloemers FW, Blokhuis TJ, Patka P, Bakker FC, Wippermann BW, Haarman HJ. Autologous bone versus calcium-phosphate ceramics in treatment of experimental bone defects. *Journal of Biomedical Materials Research* 66B, 526-531 (2003)
7. Hedberg EL, Kroese-Deutman HC, Shih CK, Crowther RS, Carney DH, Mikos AG, Jansen JA. In vivo degradation of porous poly(propylene fumarate)/ poly(DL-lactic-*co*-glycolic acid) composite scaffolds. *Biomaterials* 26, 4616-4623 (2005)
8. van Tienen TG, Heijkants RG, Buma P, de Groot JH, Pennings AJ, Veth RP. Tissue ingrowth and degradation of two biodegradable porous polymers with different porosities and pore sizes. *Biomaterials* 23, 1731-1738 (2002)
9. Jansen JA, Vehof JW, Ruhe PQ, Kroeze-Deutman H, Kuboki Y, Takita H, Hedberg EL, Mikos AG. Growth factor-loaded scaffolds for bone engineering. *Journal of Controlled Release* 101, 127-136 (2005)
10. Kaito T, Myoui A, Takaoka K, Saito N, Nishikawa M, Tamai N, Ohgushi H, Yoshikawa H. Potentiation of the activity of bone morphogenetic protein-2 in bone regeneration by a PLA-PEG/hydroxyapatite composite. *Biomaterials* 26(1), 73-79 (2005)
11. Saito N, Takaoko K. New synthetic biodegradable polymers as BMP carriers for bone tissue engineering. *Biomaterials* 24, 2287-2293 (2003)
12. Das S, Hollister SJ. Tissue engineering scaffolds. *Encyclopedia of Materials: Science and Technology*, 1-7 (2003)
13. Kokubo S, Mochizuki M, Fukushima S, Ito T, Nozaki K, Iwai T, Takahashi K, Yokota S, Miyata K, Sasaki N. Long-term stability of bone tissues induced by an osteoinductive biomaterial, recombinant human bone morphogenetic protein-2 and a biodegradable carrier. *Biomaterials* 25, 1795-1803 (2004)
14. Lieberman JR, Daluiski A, Einhorn T. The role of growth factors in the repair of bone. *The Journal of Bone and Joint Surgery* 84A(6), 1032-1044 (2002)
15. Wozney JM. Bone morphogenetic proteins. *Progress in Growth Factor Research* 1 (4), 267-280 (1989)

16. Kokubo S, Fujimoto R, Yokota S, Fukushima S, Nozaki K, Takahashi K, Miyata K. Bone regeneration by recombinant human bone morphogenetic protein-2 and a novel biodegradable carrier in a rabbit ulnar defect model
17. Wozney, JM. Overview of bone morphogenetic proteins. *Spine* 27, S2-S8 (2002)
18. Urist MR, Lietze A, Dawson E. Beta-tricalcium phosphate delivery system for bone morphogenetic protein. *Clinical Orthopaedics and Related Research* 187, 277-280 (1984)
19. Wozney JM. The bone morphogenetic protein family and osteogenesis. *Molecular Reproduction and Development* 32, 160-167 (1992)
20. Groeneveld EHJ, Burger EH. Bone morphogenetic proteins in human bone regeneration. *European Journal of Endocrinology* 142, 9-21 (2000)
21. Rodríguez-Lorenzo LM, Ferreira JMF. Development of porous ceramic bodies for applications in tissue engineering and drug delivery systems. *Materials Research Bulletin* 39, 83-91 (2004)
22. El-Ghannam A. Bone reconstruction: from bioceramics to tissue engineering. *Expert Rev. Med. Devices* 2(1), 87-101 (2005)
23. Wheeler DL, Chamberland DL, Schmitt JM, Buck DC, Brekke JH, Hollinger JO, Joh SP, Suh KW. Radiomorphometry and biomechanical assessment of recombinant human bone morphogenetic protein 2 and polymer in rabbit radius ostectomy model. *Journal of Biomedical Material Research* 43, 365-373 (1998)
24. Zabka AG, Pluhar GE, Edwards RB 3rd, Manley PA, Hayashi K, Heiner JP, Kalscheur VL, Seeherman HJ, Markel MD. Histomorphometric description of allograft bone remodeling and union in a canine segmental femoral defect model: a comparison of rhBMP-2, cancellous bone graft, and absorbable collagen sponge. *Journal of Orthopaedic Research* 19, 318-327 (2001)
25. Damien CJ, Parsons JR. Bone graft and bone graft substitutes: a review of current technology and applications. *Journal of Applied Biomaterials* 2, 187-208 (1991)
26. Sumner DR, Turner TM, Urban RM, Turek T, Seeherman H, Wozney JM. Locally delivered rhBMP-2 enhances bone ingrowth and gap healing in a canine model. *Journal of Orthopaedic Research* 22, 58-65 (2004)
27. Vehof JWM, Takita H, Kuboki Y, Spauwen PH, Jansen JA. Histological characterization of the early stages of bone morphogenetic protein-induced osteogenesis. *Journal of Biomedical Materials Research* 61(3), 440-449 (2002)
28. Jingushi S, Urabe K, Okazaki K, Hirata G, Sakai A, Ikenoue T, Iwamoto Y. Intramuscular bone induction by human recombinant bone morphogenetic protein-2 with beta-tricalcium phosphate as a carrier: in vivo bone banking for muscle-pedicle autograft. *Journal of Orthopaedic Science* 7, 490-494 (2002)
29. Yuan CA, De Bruijn JD, Zhang X, Van Blitterswijk CA, De Groot K. Use of an osteoinductive biomaterial as a bone morphogenetic protein carrier. *Journal of Materials Science: Materials in Medicine* 12, 761-766 (2001)
30. Horisaka Y, Okamoto Y, Matsumoto N, Yoshimura Y, Kawada J, Yamashita K, Takagi T. Subperiosteal implantation of bone morphogenetic protein adsorbed to hydroxyapatite. *Clincal Orthopaedics and Related Research* 268, 303-312 (1991)
31. Eggli PS, Muller W, Schenk PK. Porous hydroxyapatite and tricalcium phosphate cylinders with two different pore size ranges implanted in the cancellous bone of rabbits. A comparative histomorphometric and histologic study of bony ingrowth

and implant substitution. *Clincal Orthopaedics and Related Research* 232, 127-137 (1988)
32. Fujishiro Y, Oonishi H, Hench LL. Quantitative comparison of *in vivo* bone generation with particulate Bioglass®. *Bioceramics* 10, 283-286 (1997)
33. El-Ghannam A. Advanced bioceramic composite for bone tissue engineering: design principles and structure-bioactivity relationship. *Journal of Biomedical Materials Research* 69A, 490-501 (2004)
34. Gao TJ, Lindholm TS, Kommonen B, Ragni P, Paronzini A, Lindholm TC. Microscopic evaluation of bone-implant contact between hydroxyapatite, bioactive glass and tricalcium phosphate implanted in sheep diaphyseal defects. *Biomaterials* 16, 1175-1179 (1995)
35. Sachlos E, Reis N, Ainsley C, Derby B, Czernuszka JT. Novel collagen scaffolds with predefined internal morphology made by solid freeform fabrication. *Biomaterials* 24, 1487-1497 (2003)
36. Rai B, Teoh SH, Ho KH, Hutmacher DW, Cao T, Chen F, Yacob K. The effect of rhBMP-2 on canine osteoblasts seeded onto 3D bioactive polycaprolactone scaffolds. *Biomaterials* 25, 5499-5506 (2004)
37. Chen Z, Li D, Lu B, Tang Y, Sun M, Xu S. Fabrication of osteo-structure analogous scaffolds via fused deposition modeling. *Scripta Materialia* 52, 157-161 (2005)
38. Leong KF, Cheah CM, Chua CK. Solid freeform fabrication of three dimensional scaffolds for engineering replacement tissues and organs. *Biomaterials* 24, 2363-2378 (2003)
39. Kokubo T, Kushitani H, Sakka S. Solutions able to reproduce *in vivo* surface-structure changes in bioactive glass-ceramic A-W^3. *Journal of Biomedical Materials Research* 24, 721-734 (1990)
40. Tancred DC, McCormack BAO, Carr AJ. A synthetic bone implant macroscopically identical to cancellous bone. *Biomaterials* 19, 2303-2311 (1998)
41. Klawitter JJ, Hulbert SF. Application of porous ceramics for the attachment of load bearing internal orthopedic applications. *Journal of Biomedical Materials Research* 5(6), 161-229 (1971)
42. Lu JX, Flautre B, Anselme K, Hardouin P, Gallur A, Descamps M, Thierry B. Role of interconnections in porous Bioceramics on bone recolonization *in-vitro* and *in-vivo. Journal of Materials Science: Materials in Medicine* 10(2), 111-120 (1999)
43. Ruhe PQ, Hedberg EL, Padron NT, Spauwen PH, Jansen JA, Mikos AG. rhBMP-2 release form injectable poly(DL-lactic-co-glycolic acid)/calcium-phosphate cement composites. *The Journal of Bone and Joint Surgery* 85, 75-81 (2003)
44. Ruhe PQ, Kroese-Deutman HC, Wolke JG, Spauwen PH, Jansen JA. Bone inductive properties of rhBMP-2 loaded porous calcium phosphate cement implants in cranial defects in rabbits. *Biomaterials* 25, 2123-2132 (2004)
45. El-Ghannam A, Ning CQ, Mehta J. Cyclosilicate nanocomposite: a novel resorbable bioactive tissue engineering scaffold for BMP and bone-marrow cell delivery. *Journal of Biomedical Materials Research* 71A(3), 377-390 (2004

46. Gu YW, Khor KA, Cheang P. Bone-like apatite layer formation on hydroxyapatite prepared by spark plasma sintering (SPS). *Biomaterials* 25(18), 4127-4134 (2004)
47. Ding SJ, Ju CP, Lin C. Morphology and immersion behavior of plasma-sprayed hydroxyapatite/bioactive glass coatings. *Journal of Materials Science: Materials in Medicine* 11, 183-190 (2000)
48. Lo WJ, Grant DM. Hydroxyapatite thin films deposited onto uncoated and (Ti,Al,V)N-coated Ti alloys. *Journal of Biomedical Materials Research* 46(3), 408-417 (1999)
49. Zhou J, Zhang X, Chen J, Zeng S, De Groot K. High temperature characteristics of synthetic hydroxyapatite. *Journal of Materials Science: Materials in Medicine* 4, 83-85 (1993)
50. Jones JR, Sepulveda P, Hench LL. Dose-dependent behavior of bioactive glass dissolution. *Journal of Biomedical Materials Research* 58(6), 720-726 (2001)
51. Nordstrom EG, Karlsson KH. Carbonate-doped hydroxyapatite. *Journal of Materials Science: Materials in Medicine* 1, 182-184 (1990)
52. Méndez JA, Fernandez M, Gonzalez-Corchon A, Salvado M, Collia F, de Pedro JA, Levenfeld BL, Lopez-Bravo A, Vazquez B, San Roman J. Injectable self-curing bioactive acrylic-glass composites charged with specific anti-inflammatory/analgesic agent. *Biomaterials* 25(12), 2381-2392 (2004)
53. Kokubo T, Kim H, Kawashita M. Novel bioactive materials with different mechanical properties. *Biomaterials* 24(13), 2161-2175 (2003)
54. Oliveira AL, Malafaya PB, Reis RL. Sodium silicate gel as a precursor for the *in vitro* nucleation and growth of a bone-like apatite coating in compact and porous polymeric structures. *Biomaterials* 24(15), 2575-2584 (2003)
55. Miyaji F, Kim HM, Handa S, Kokubo T, Nakamura T. Bonelike apatite coating on organic polymers: novel nucleation process using sodium silicate solution. *Biomaterials* 20, 913-919 (1999)
56. Liu X, Ding C, Chu P. Mechanism of apatite formation on wollanstonite coatings in simulated body fluids. *Biomaterials* 25(10), 1755-1761 (2004)
57. Seto I, Asahina I, Oda M, Enomoto S. Reconstruction of the primate mandible with a combination graft of recombinant human bone morphogenetic protein-2 and bone marrow. *Journal of Oral Maxillofacial Surgery* 59, 53-61 (2001)

VITA

Amanda Peter Hart was born in Louisville, Kentucky in 1981. She grew up in Oldham County where she excelled in sports all her life. She attended the University of Kentucky in 1999 where she received her Bachelors of Science in Mechanical Engineering in 2003. As an undergraduate, Amanda was an officer of Phi Sigma Rho, an engineering and social sorority. In 2003, she began her Master's Degree work in Biomedical Engineering at the University of Kentucky. As a graduate student, she presented her work at the Society for Biomaterials conference in Philadelphia, PA. She was also an officer of the local chapter of the Biomedical Engineering Society.